



Optical Fiber Sensors: A Versatile Technology Platform for Sensing

Bishnu P. Pal

Abstract | Optical fibers are now taken for granted as signal transmission media for telecommunication and the Internet. Optical fibers also provide a versatile platform for sensing a host of physical and chemical effects, and parameters of interest. Though optical techniques for measurements were well known for a long time, utility of optical fibers for sensing and measurements has been recognised and widely appreciated only in the last two to three decades. It has indeed become a subject of intense activity over recent times due to a variety of attractive features, notably their immunity to electromagnetic interference, enabling distributed sensing, and remote collection of sensed data for post processing owing to their compatibility to optical fiber telemetry. Fiber optics offers a versatile platform for realizing a multitude of sensors for a variety of applications in areas as broad as civilian, defence, biomedical, and so on. Functional principles of some of these sensors could be extremely simple, while some sensors could be ultra-sensitive that could yield extremely small magnitudes of certain measurands. This article is an attempt to review the basic principles that underpin this area of research and expose the readers to few such fiber optical sensors by describing their applications.*

1 Introduction

In recent years, the applicability of optical measurement techniques in the area of instrumentation and sensors has seen a prolific growth with the ready availability of low-loss optical fibers and associated optoelectronic components. Fiber Optic (FO) waveguide offers certain key advantages over conventional electronic sensors, namely, signals transported via optical fibers are immune to Electromagnetic Interference (EMI) and Radio Frequency Interference (RFI) owing to the dielectric nature of fibers, and are intrinsically safe in explosive environments such as on-shore

and off-shore oil and petroleum fields with no risk of fire/sparks, high voltage insulation and absence of ground loops, and hence obviate any necessity of isolation devices like opto-couplers. Furthermore, a fiber is chemically inert, has low volume and weight (a kilometer of 200- μm thick silica fiber weighs approximately 70 gm and occupies a volume of $\sim 30 \text{ cm}^3$), and owing to its low physical footprint and mechanical flexibility, can be used to sense normally inaccessible regions (such as intra-body cavities for biomedical applications) without perturbation of the transmitted signals. FO sensors are potentially resistant to nuclear or ionizing radiations, and can be easily interfaced with low-loss telecom grade optical fibers for remote sensing and measurements, for which the control electronics for LED/laser and detectors can easily be located far away (can be of the order of tens of kilometers) from the sensor head. The inherent large bandwidth of an optical

*The article is to a large extent adapted from a book chapter "Optical Waveguide Sensors" that I wrote for the upcoming book "Handbook of Optical Sensors" ed by José Luis Santos and Faramarz Farahibeing published by CRC Press/Taylor & Francis Group, LLC. ISBN: 9781439866856.

fiber supports the capability of multiplexing a large number of individually addressed point sensors in a fiber network for distributing sensing, i.e. continuous sensing along the length of the fiber. By exploiting these features, fibers are readily employed in chemical and process industries, health monitoring of civil structures, biomedical instrumentation and many more areas, and have attracted intensive research and development efforts globally, for developing fiber optic sensors. This has led to the emergence of a plethora of FO sensors for accurate sensing and measurement of physical parameters and fields, such as pressure, temperature, liquid levels, refractive indices of various fluids, pH, electric current, rotation, displacement and acceleration, acoustic, electric and magnetic fields, and so on. The initial developmental work was concentrated predominantly on military applications such as fiber optic hydrophones for submarine and under-sea applications, and gyroscopes for marine vessels, missiles and aircrafts. These early applications were subsequently followed by a large number of civilian applications.¹ The 1970s became a watershed decade for fiber optic telecommunications when the development of the first low-loss (<20 dB/km) high-silica optical fiber was reported² concomitantly with that of semiconductor laser diodes that could be operated at room temperatures for long hours without degradation as well as high-efficiency photo detectors. It was discovered that the transmission behaviour of optical fibers exhibited a strong sensitivity towards certain external perturbations such as microbends, pressure etc. At the time, significant efforts were invested into reducing the sensitivity of signal-carrying optical fibers to external effects by developing design strategies involving fiber refractive index profiles and cabling geometries. **An alternate school of researchers took advantage of these observations and started to exploit this sensitivity for representing a variety of measurands to develop a fiber optic platform for configuring sensing devices.** Today, FO sensors play a major role in industrial, medical, aerospace, and consumer applications.

This article describes a variety of FO sensors and their underlying functional principles with applications as a versatile sensor technology platform. As is well known, an optical fiber represents an optical waveguide with a cylindrical geometry having a central core of refractive index n_1 , surrounded by a cladding of a different refractive index n_2 ($n_2 < n_1$) as shown in Figure 1. Typical dimensions of an optical fiber for the core is 50 – 100/200 μm (multimode fibers) and 4–10 μm (depending on

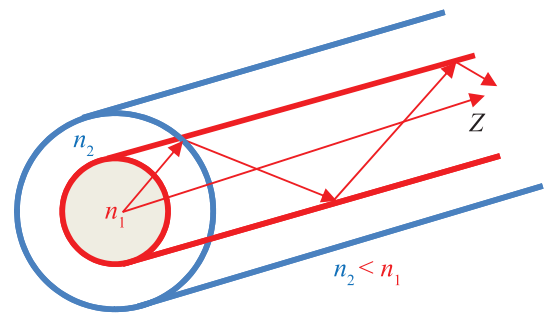


Figure 1: Optical fiber waveguide geometry; core of refractive index (r. i.) n_1 surrounded by a cladding of r. i. $n_2 < n_1$.

operating wavelength) for single-mode fibers, while the overall diameter could be 80–600 μm depending on applications and sensing device; for telecommunication applications standard overall fiber diameter is $125 \pm 1 \mu\text{m}$. Usually large diameter fibers are plastic clad silica fibers. Refractive index contrast in terms of relative core cladding index difference [$\Delta = (n_1 - n_2)/n_1$] is 0.35–1%, depending on type of the fiber and their intended use for specific applications.

2 FO Sensor Classification

Broadly, a fiber optic sensor may be classified as either *intrinsic* or *extrinsic*.³ In an intrinsic sensor, the physical parameter/effect to be sensed modulates the transmission properties of the sensing fiber, whereas in an extrinsic sensor the modulation takes place outside the fiber, as shown in Figure 2. In the former, one or more of the physical properties of the guided light, e.g., intensity, phase, polarization, and wavelength/colour is modulated by the measurands, while in the latter case, the fiber merely acts as a conduit to transport the light signal from the sensor head to a photo detector/optical power meter for detection and quantitative measurement.

FO sensors rely on intensity modulation, interferometry or phase modulation, fluorescence, and spectral modulation of the light used in the sensing process. Figure 3 is a representative figure in terms of algebraic interpretation of these different modulation schemes. However, out of these, the intensity and phase modulated techniques offer the widest spectrum of FO sensors. Intensity modulation can be achieved through a variety of schemes, e.g., displacement of one fiber relative to the other, shuttering, i.e. variable attenuation of light between two sets of aligned fibres, collection of modulated light reflected from a target exposed to the measurand and loss modulation of light in the core or in the cladding through bending,

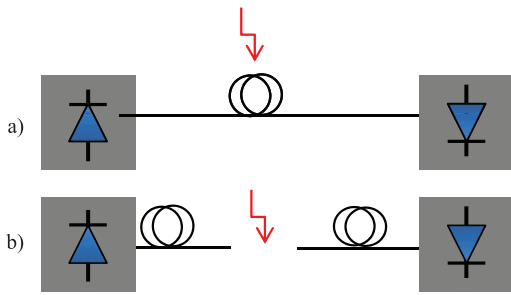
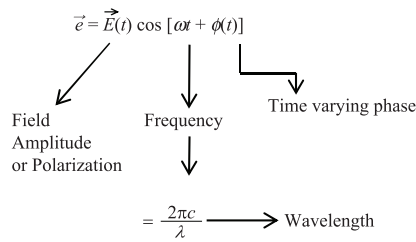


Figure 2: Examples of a) intrinsic b) extrinsic fiber sensor; in the intrinsic sensor the measurands induce modulation of one of the characteristics of the guided light while in extrinsic sensors the measurands-induced modulation of light takes place outside the fiber, as here in the gap between the two fibers. Measurand is debugged by the detector/power meter.



Intensity modulated sensors: $E(t) \cos[\omega t + \phi(t)]$

Phase modulated sensors: $E(t) \cos[\omega t + \phi(t)]$

Polarization modulated sensors: \vec{E}

Wavelength modulated sensors: $E(\lambda) \cos[\omega t + \phi(\lambda)]$

Figure 3: Algebraic interpretation of different modulation schemes.

microbending, or evanescent coupling to another fiber/medium. The advantage of intensity modulated sensors lies in their simplicity of construction and compatibility with multimode fiber technology (which offers enhanced transmission as it supports multiple field distributions). Phase modulated FO sensors require an interferometric measurement set-up, which is usually complex in its lay out requiring isolation of the reference arm/path from the measurand, although, as we shall see later in the article, they theoretically offer orders of magnitude higher sensitivity as compared to intensity modulated sensors.

3 Intensity Modulated FO Sensors

Intensity modulated fiber optic sensors are the most widely studied FO sensors.^{1,4-6} The general configuration of an intensity modulated sensor can be understood from Figure 4, in which the baseband signal (the measurand) modulates the

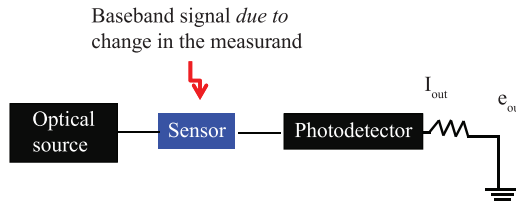


Figure 4: General principle of an intensity modulated fiber optic sensor, in which I_{out} represents modulated optical output and e_{out} is the modulation envelope in the detected voltage output.

intensity of the light propagating through the fiber acting as the sensor head. The resultant modulation envelope is reflected in the voltage output of the detector, which upon calibration, can be used to retrieve the magnitude of the measurands.

A generic classification of intensity-modulated fiber optic sensors is schematically depicted in Figure 5. It shows an example of signal from an input fiber undergoing a measurand-induced variable attenuation as it is transmitted to a receiving fiber. The figure also depicts a generic example of light from a source, which undergoes measurand-induced modulation either through reflection from a diaphragm subjected to a variable pressure environment or through reflection/scattering from a chemical environment such as a turbid or a fluorescing solution.

An important aspect that needs to be addressed in all intensity modulated sensors is the compensation for any variations/fluctuations in the intensity of the light source used during the measurements. This can easily be accounted for by obtaining a reference measurement by tapping a small portion of the source intensity via a fiber coupler to enable continuous monitoring of the source by a photodetector/power meter. Common mode fluctuations are rejected by taking the ratio of the measurand-induced variations in light intensity with respect to this reference intensity.

Measurand-induced modulations of light coupling across a gap between two fibers is exploited for detecting pressure, sound waves, liquid levels, and so on. In its simplest form as shown in Figure 5, an interceptor, typically in the form of a knife-edge mounted on the diaphragm acting as the lid of a pressure chamber, can be used to detect whether the pressure has exceeded a pre-determined threshold value through suitable calibration. Optical fiber microswitches based on this basic principle are now commercially available for detection of displacement (e.g. with pressure release valves) in hazardous environments.⁷ Similarly, if the level of a liquid exceeds a pre-determined threshold level/height at which

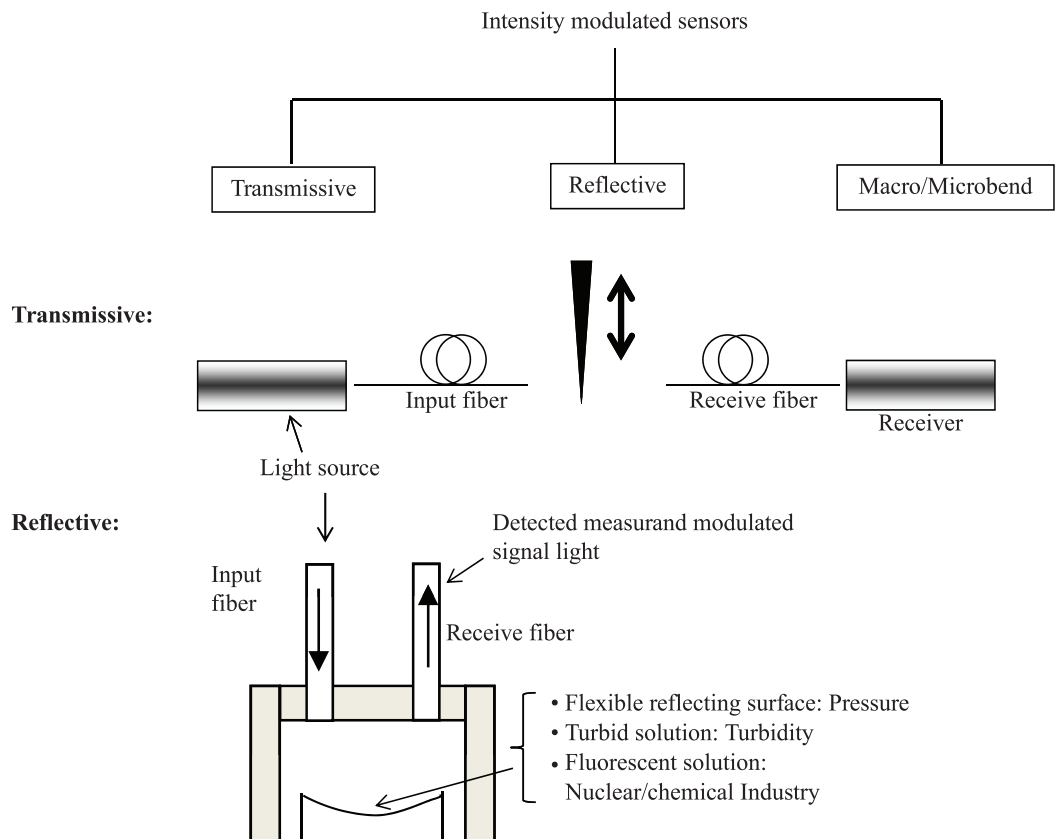


Figure 5: Classification of intensity modulated sensors: (1) measurand-induced modulation of transmitted light across a gap between two fibers; (2) measurand-induced modulation of reflected light from a flexible reflector covering a pressure environment or a fixed reflector at the end of a turbid or a fluorescing solution.

two fibers are kept perfectly aligned with a small (\sim few μm) air gap in between from the wall of the liquid tank/container at a specific height by integrating an alarm signal trigger mechanism, corrective action is taken as soon as the liquid level rises to that height. This configuration is particularly attractive if the liquid happens to be a potential fire hazard like gasoline, as no electric sparks must occur during the measurement process. In an alternative version, sound and displacement are detected by mounting one of two fibers on an acoustically driven vibrating base/holder with a small length of the fiber extending from its holder as a cantilever, while the other is kept fixed on a stable base. Initially, both fibers are kept perfectly aligned by maximizing the power throughput across the air gap in between them. In the presence of acoustic waves, the associated vibration modulates the light transmittance across the two fibers, which is subsequently decoded to yield the frequency of the acoustic wave. When one fiber is displaced with respect to the other by one core diameter, approximately 100% light intensity modulation occurs. **Approximately, the first**

20% of displacement yields a linear output.⁵ In the original experiment involving this configuration (Spillman *et al.* 1980), the device could detect deep-sea noise levels in the frequency range of 100 Hz to 1 kHz and transverse static displacements down to a few Angstrom. For higher accuracy measurements,⁸ two opposed gratings were used (as shown in Figure 6) in a configuration, wherein one was mounted on a flexible rubber diaphragm on which the acoustic waves were incident and the other mounted on the rigid base plate of the housing. These gratings were made on two $9 \times 3 \times 0.7 \text{ mm}^3$ cover strip glass substrates on which a 1.16 mm square grating pattern was produced from a $5 \mu\text{m}$ strip mask by means of photoresist lift off technique through 1200 \AA evaporation of chromium. An index matching liquid was inserted between the gratings, which were aligned such that they were parallel and displaced relative to each other by one half strip widths to ensure operation of the sensor at the maximum of the linear sensitivity region. The overlapped region of the two glass slides was sealed with a soft epoxy, which enabled displacement of one grating relative to the

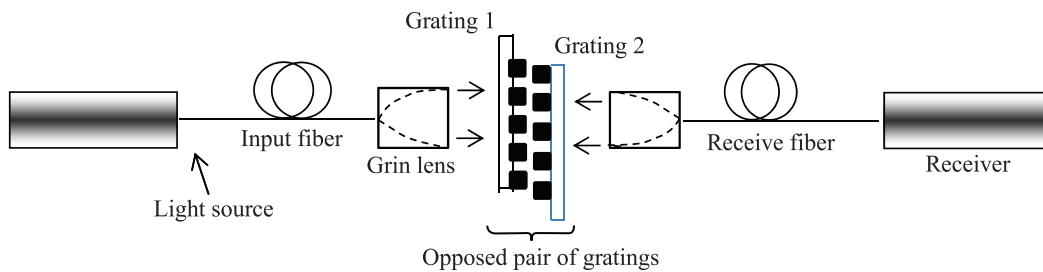


Figure 6: Schematic of an acoustic field/pressure sensor based on opposed gratings placed within the gap between a pair of multimode fibers, grating 1 (attached to a diaphragm) is movable by the measurand relative to the grating 2 (fixed to a base); a pair of GRIN microlenses were used to collimate light (from input fiber) and focus (in to receiving fiber) (after Ref. [8]).

other and also provided an elastic restoring force. Light from a He-Ne laser was launched into a plastic, 200- μm core input fiber whose output was collimated by a GRIN Selfoc lens bonded to it. This collimated beam, after transmission through the grating assembly, was refocused by means of a second GRIN lens onto the input end of the receiving fiber (also plastic). The resultant device was sensitive to acoustic pressures less than 60 dB (relative to 1 μ pascal) over a 100 Hz to 3 kHz frequency range and could resolve relative displacements as small as few Angstroms with a dynamic range of 125 dB. It was relatively insensitive to static pressure and responded well to variations in a.c. pressure for use as a hydrophone.

In reflective FO sensors, the measurand induces modulation of the light reflected from a reflecting surface. In its simplest form, a Y-coupler fiber optic probe, consisting of two multimode fibers cemented/fused along some portion of their length (two bundles of fibers may also be substituted in their place) to form a power divider, constitutes a reflective FO sensor. If light is injected through port 1 of the Y-power divider on to a reflecting diaphragm and the back reflected light exits through port 3, its intensity depends on the distance of the reflecting target from the fiber probe as shown in Figure 7. The dynamic range of such sensors can be enhanced by the use of a lens between the fiber probe and the reflective target. Such sensors are used to detect displacement, pressure or even the position of a float in a variable area flow meter.⁴ The use of such reflective FO sensors have been demonstrated for determining surface texture,⁹ flow rates (in the range ~ 1 –10 m/sec) of pulp suspensions in tubes,¹⁰ pressures over a range of ~ 100 psi,¹¹ in medical catheters as inter-cardiac pressure transducers with a sensitivity ~ 1 mm of Hg and linearity in the range of 0–200 mm of Hg,^{12,13} vibrations,^{14,15} and also as a fiber laser Doppler anemometer (fiber LDA).¹⁶

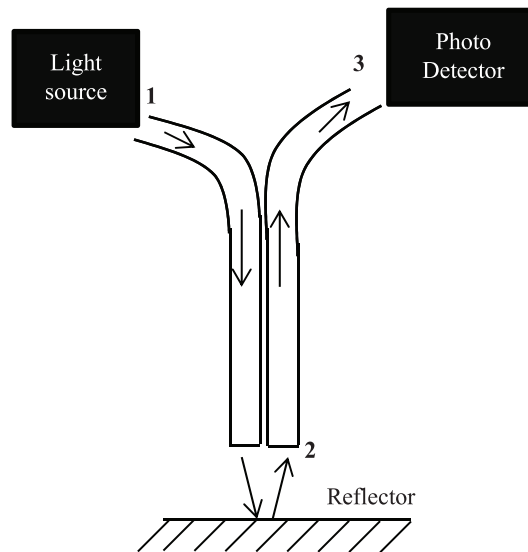


Figure 7: Schematic of a reflective sensor in which one fiber/a bundle of fibers transmits light from a source at port 1 to a reflecting surface and another fiber/fiber bundle collects the reflected light at port 2 as a conduit for detection by a detector at port 3.

The phenomenon of frustrated total internal reflection (FTIR) forms the underlying basis of a fiber optic-based threshold liquid level sensor as shown in Figure 8. Light is coupled into a fiber, which is cemented with an optical adhesive at one end of the base of a 90° glass micro-prism and a second fiber is optimally fixed at the other end of the prism base for collecting total internally reflected light. As the level of the liquid rises and touches the prism, FTIR takes place resulting in a dramatic reduction of light received by the second fiber (as registered by the power meter). This sensor configuration can be used to trigger an alarm signal once a predetermined liquid level is reached (in tanks and reservoirs for instance) to indicate

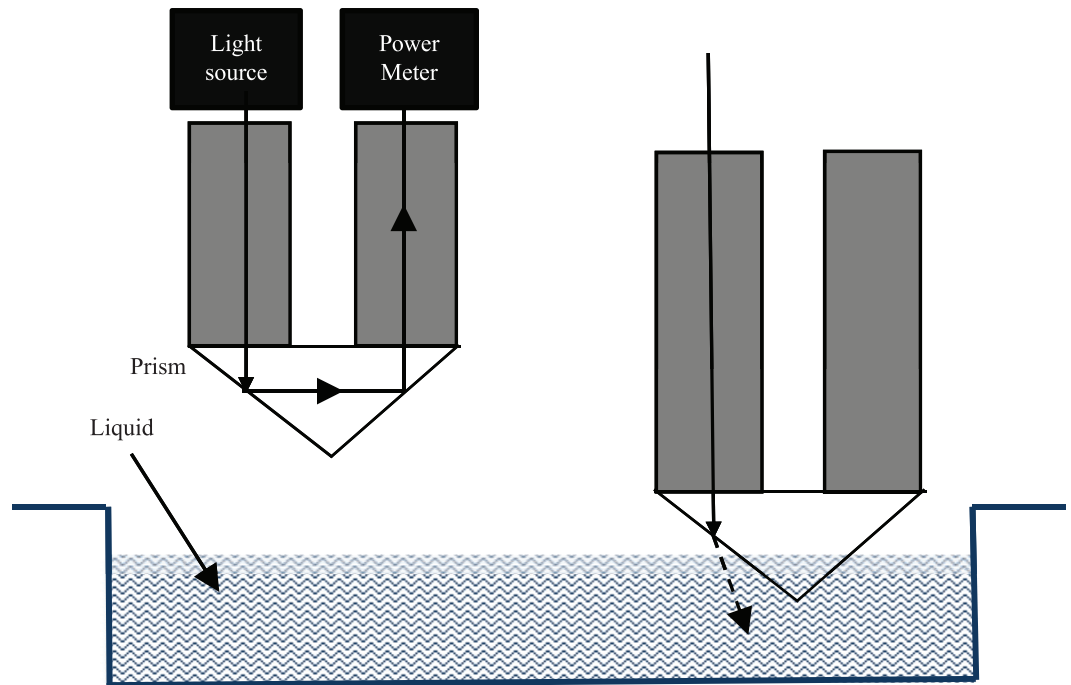


Figure 8: Schematic of a liquid level sensor, whose working principle is based on frustrated total internal reflection as described in the text.

when sufficient liquid levels have been achieved and avoid spillage.

Extrinsic perturbations such as bends on a fiber's lay lead to transmission loss [see Fig. 9a]. This effect needs to be accounted for while laying a fiber for use in a telecommunication link so that no tight bends are encountered by the fiber. A simple experiment involving launching visible laser light into a fiber when it is kept straight and when the same fiber is bent in the shape of a circle (e.g. by introducing a tight bend in a fiber lay through a loop around one's finger) would immediately reveal that a fiber suffers radiation losses at bends. This can be understood by acknowledging that the fractional modal power travelling in the cladding along the periphery of a bent fiber would be required to travel at a rate faster than the local plane wave velocity of light in order to maintain equi-phase fronts across radial planes. Since this is physically not possible, part of the modal field radiates away.¹⁷ In contrast to bend-induced transmission losses due to constant curvatures, if the fiber lay goes through a succession of very small bends [see Figure 9b], the fiber exhibits transmission loss due to what is referred to as microbend-induced loss in a fiber.

Physically, microbending leads to a redistribution of power amongst the modes of the fiber and also transfers a fraction of the power from certain high order guided modes to radiation modes

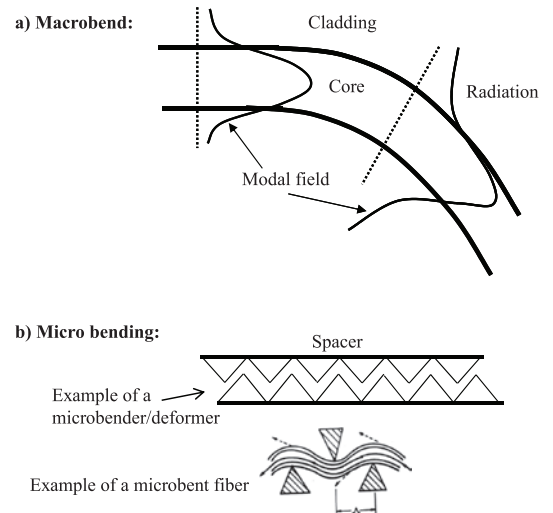


Figure 9: Schematic illustration of a) macrobend and b) microbend intensity modulated fiber optic sensor; Λ represents spatial wavelength of a microbender.

leading to a loss in throughput power. Through a theoretical coupled mode analysis, it can be shown that strong coupling between the p th and q th mode of a fiber occurs if $\Delta\beta = |\beta_p - \beta_q|$ matches the spatial wave number ($= 2\pi/\Lambda$) of the microbending deformer. This phenomenon is exploited for detection in a variety of FO sensors. Initially, these sensors were used as hydrophones and displacement

sensors. Depending on the configuration of the microbender, the same phenomenon is used for constructing FO sensors which determine changes in parameters such as temperature, acceleration, electric and magnetic fields.¹⁸ For example, to function as a temperature sensor, the deformer needs to be made from metal; for electric field, it should be a piezoelectric material; for magnetic fields, a magnetostrictive material, etc. The minimum detectability of different environmental changes achievable in fiber microbend sensors is tabulated in Table 1.¹⁸

An interesting application of microbend sensors is for chemical sensing and involves an Optical Time Domain Reflectometer (OTDR) shown in Figure 10, which is used extensively in the telecom industry for distributed monitoring of the overall condition of an existing optical telecommunication network (e.g. detect fiber breaks, localized excessive bends or microbends across the fiber link, length of the link etc.).

Figure 11a represents a schematic of the fiber cable configuration. These cables are tailored for distributed microbend sensing. A specific polymer material in the form of a gel, which swells

when water ingresses into it, for example, surrounds a central GRP rod; this combination is held along its length within the cable along with a multimode optical fiber by helically wrapping a Kevlar rope around the polymer. This overall combination is held within a protective sheath having micro-pores. When there is water spillage anywhere along the cable lay, water penetrates into the cable through its pores, and the chemically active hydrogel swells due to the absorption of water. This induces localized microbending of the fiber within the cable as shown in Figure 11b, resulting in loss at the spill location, which is then instantly captured in the OTDR trace as shown in Figure 11c. The same principle can be employed to detect spillage of other liquids (petrol, kerosene, diesel, crude oil) like gasoline, if the hydrogel is substituted by another appropriate substance.

The excitation and collection of fluorescence from fibers is another example of FO chemical sensing, as depicted schematically in Figure 12. Since fluorescence is characteristic of a material, its spectroscopic measurement yields information about the presence and its concentration in a solution. Fiber optic probes of various designs are used in such measurements. These probes are also referred to in the literature as “optrodes”.

A generic schematic of an optrode-based optical sensing approach based on fluorescence measurements is shown in Figure 13a, and few examples of optrode cross-sections are shown in Figure 13b. Optrode-based sensing techniques find applications in biomedical optics for detection of cancerous cells, diagnostics and monitoring of

Table 1: Minimum detectability of environmental changes.

Environment	Minimum detectability
Pressure	3×10^{-4} dyne/cm ²
Temperature	4×10^{-6} °C
Magnetic field	9.6×10^{-5} Oe
Electric field	1.7×10^{-1} V/m

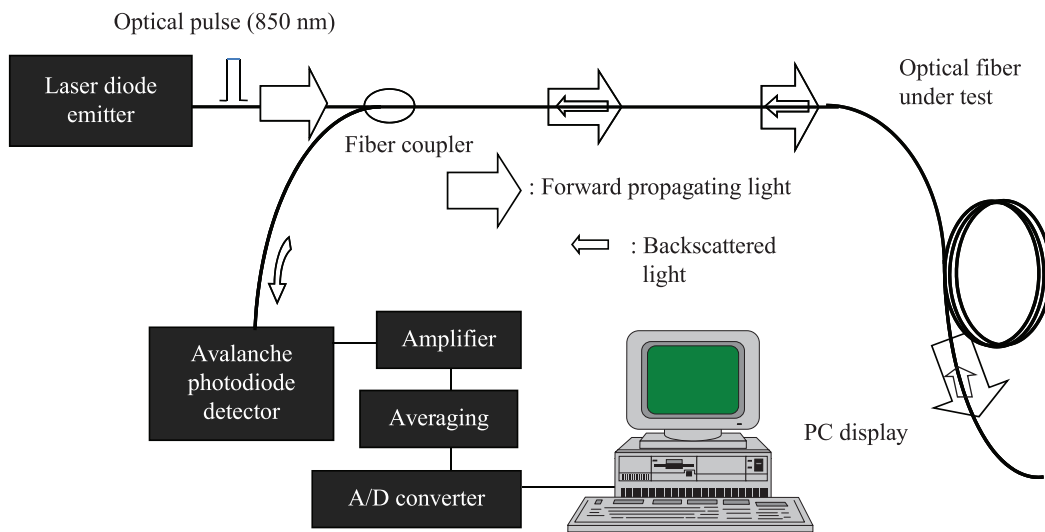


Figure 10: Schematic of an OTDR-based microbend intensity modulated fiber optic sensor (figure courtesy B. Culshaw, EEE Department, University of Strathclyde, Glasgow, UK).

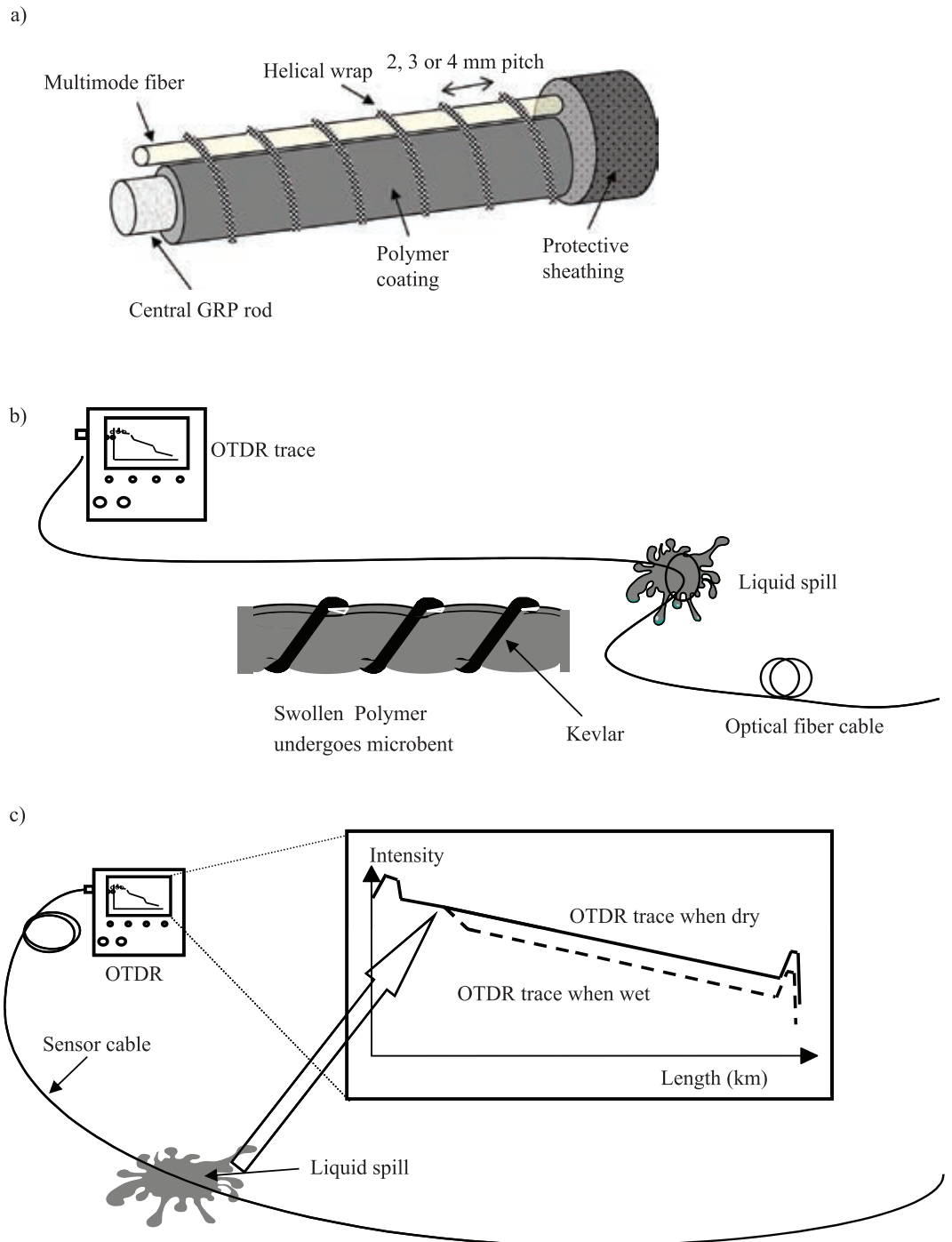


Figure 11: a) Schematic of the fiber cable configuration for microbent fiber optic sensor; b) portion of the microbent fiber cross-section due to swelling of the polymer due to water or liquid chemical ingress, and the resultant OTDR trace from the fiber; c) Schematic of the OTDR trace from the sensing fiber cable under dry and wet conditions (figure courtesy B. Culshaw, EEE Department, University of Strathclyde, Glasgow, UK).

anatomical sites, etc., while in chemical industries these are useful in hazardous and aggressive environments (acidic, nuclear, inflammable).

Similar optrodes can also be used as reflective sensors mentioned earlier by using the central fiber for illuminating the sample and collecting

the reflected light from the sample through the peripheral fibers. Likewise, these can be deployed to measure scattered light from a solution such as for turbidity measurements. In a turbidity sensor configuration (see Figure 14) reported in Ref. [19], scattered light from a turbid solution

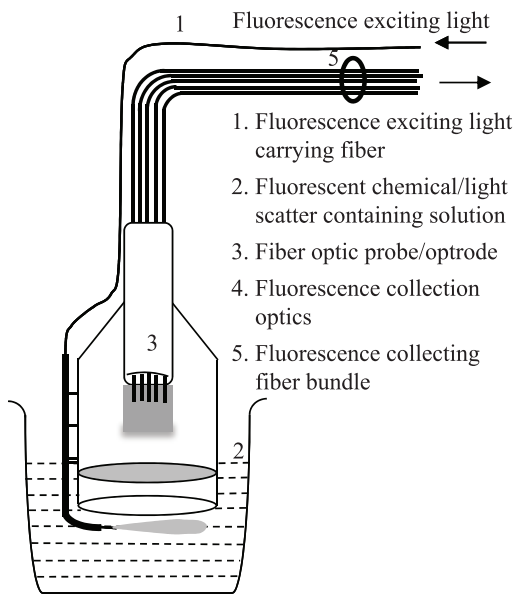


Figure 12: Schematic example of a fiber optic fluorescence sensor (personal communication, Prerana).

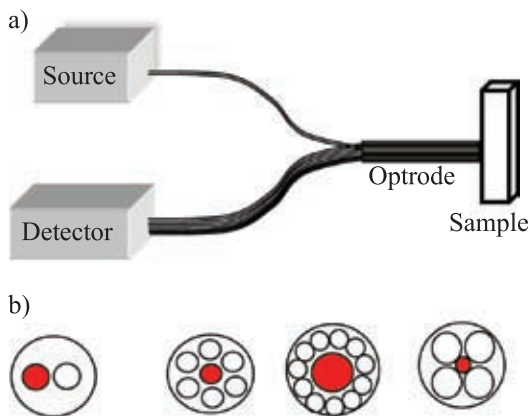


Figure 13: Schematic of a) a fiber optic fluorescence sensor, in which fluorescence is excited and collected via an optrode; b) examples of few possible variations in the optrode cross-section, illuminating fiber is indicated as filled circles (in red colour) and light collecting fibers are represented through open circles.

was collected after reflection from a concave mirror. The turbidity of a specific solution can be estimated in terms of *total interaction coefficient*, which is defined as the sum of the absorption and scattering coefficients.

The performance of this sensor, evaluated through extensive Monte Carlo simulations [see Figure 15a], with reference to the experimental set up (shown in Figure 14) and corresponding experimental results (Figure 15b) can be found in Ref. [19]. Turbidity is

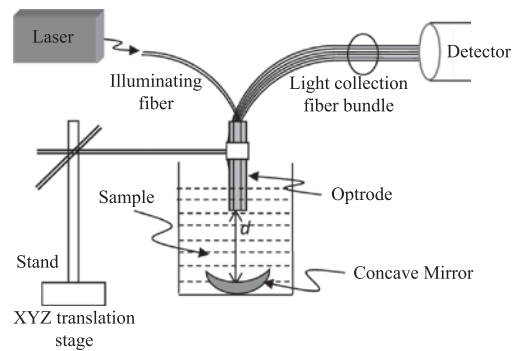


Figure 14: Schematic of the experimental set-up to collect the scattered light from the samples (Prerana *et al.* 2012); distance d between concave mirror and the optrode tip is variable.

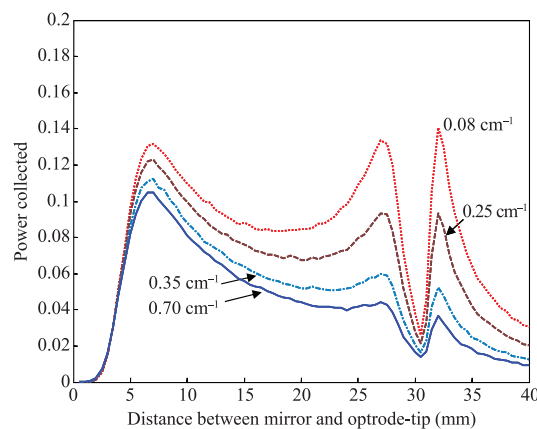


Figure 15a: Monte Carlo simulation results for collected power as a function of d for different turbid solution samples, each characterized by different interaction coefficient (μ_t), which labels the different curves (After Ref. [19] © IEEE).

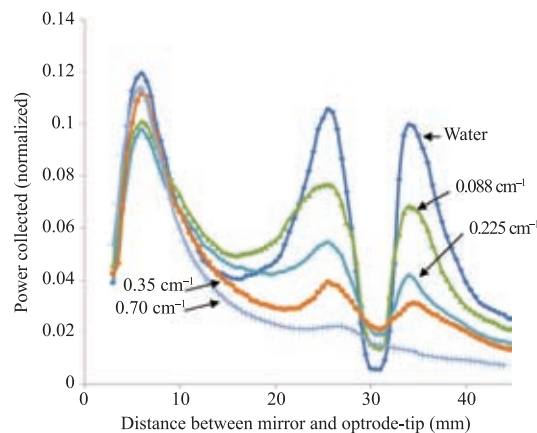


Figure 15b: Experimental results for collected power as a function of d for different turbid solution samples, each characterized by different interaction coefficient (μ_t), which labels the different curves (After Ref. [19] © IEEE).

an important indicator for checking the quality of various liquids such as water, olive oil,²⁰ etc.

The measurement of refractive index is important for many chemical industries. A multimode fiber-based refractometer reported in Ref. [21] is based on a plastic clad silica core multimode fiber having a small tapered section. Figure 16 represents the geometry of the tapered fiber.

The tapered portion can be thought of as two interconnecting fibers (referred to as Fibers 1 and 2) having core diameters $2a_{in}$, $2a_o$ ($a_o < a_{in}$) respectively. Fibers #1, #2, as well as the tapered interconnecting zone, all have the same core and cladding refractive indices n_1 and n_2 , respectively, except for the initial section of Fiber #1, in which the cladding index is n_{cl} , i.e. the plastic cladding material. A guided mode of effective index n_{e1} ($= n_1 \cos\theta_1$, θ_1 being the characteristic mode propagation angle) in Fiber #1 gets transformed to a corresponding characteristic mode effective index n_{e2} in Fiber #2 as²¹

$$n_{e2} = \left[n_1^2 - R^2 (n_1^2 - n_{cl}^2) \right]^{\frac{1}{2}} \quad (1)$$

where $R (= a_{in}/a_o)$ is the taper ratio. For a mode to be guided in Fiber #2, one requires

$$n_{e1} \geq \left[n_1^2 - \frac{n_1^2 - n_L^2}{R^2} \right]^{\frac{1}{2}} \equiv n_{e1}^{\min} \quad (2)$$

If P_o represents the total power injected into the guided modes of Fiber #1, then the power in the modes with $n_{e1} > n_{e1}^{\min}$ would be given by

$$P_b = P_o \frac{n_1^2 - n_L^2}{R^2 (n_1^2 - n_{cl}^2)} \quad (3)$$

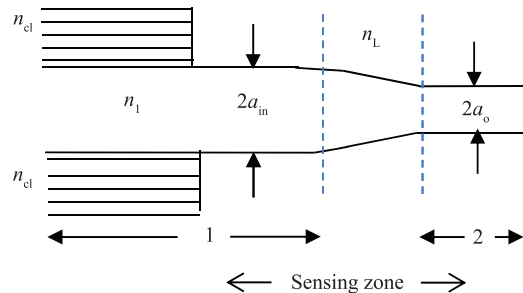


Figure 16: Refractometer based on a tapered multimode fiber (After Kumar *et al.* 1984 © IEE).

Thus, it is evident from Eq. (3) that power coupled to Fiber #2 through the taper increases linearly with proportional decrease in n_L^2 . This result has been exploited to construct a fiber refractometer based on a plastic-clad silica core fiber by removing a small portion of the plastic cladding and converting the bare fiber section into a taper by heating and stretching in a flame burner. The tapered zone was then immersed in a liquid of refractive index n_L ($< n_1$). By immersing the taper subsequently in other liquids, (and carefully cleaning the tapered zone each time), and monitoring the corresponding power reaching Fiber #2, a calibration curve was generated for the fiber taper and it can be shown²¹ that P_b decreases linearly with n_L^2 . In principle, the same technique may be exploited to construct fiber optic temperature sensors by surrounding the taper with a thermo-optic liquid (whose refractive index varies with temperature) in a metallic encapsulation. In fact, plastic clad silica fibers provide an excellent platform for a range of intensity modulated fiber optic sensors.

Side Polished Single-Mode Fiber (SP-SMF) half-coupler is another versatile sensor technology platform, in which phase resonant evanescent coupling of the SP-SMF with a Multimode Overlay Waveguide (MMOW) forms the basis of operation as a sensor. A high sensitive temperature sensor based on evanescent field coupling between a Side-Polished Fiber Half-Coupler (SPFHC) and a thermo-optic Multimode Overlay Waveguide (MMOW) was designed and realized²² (see Figure 17).

This device as such essentially functions as an asymmetric directional coupler with a band-stop characteristic attributable to the wavelength-dependent resonant coupling between the mode of the SPFHC and one or more modes of the MMOW. The wavelength sensitivity of the device was ~ 5.3 nm/°C within the measurement range of 26–70°C; this sensitivity is more than 5 times higher compared to earlier reported temperature sensors of this kind. The SPFHC was fabricated by selective polishing of the cladding from one side of a bent telecommunication standard single-mode fiber and the MMOW was formed on top of the SPFHC through spin coating. A semi-numerical rigorous normal mode analysis was employed at the design stage by including the curvature effect of the fiber lay in the half-coupler block and the resultant z -dependent evanescent coupling mechanism. The agreement between theoretical and experimental results was excellent. The temperature range measurable by this sensor was limited by the thermo-optic overlay material used; other

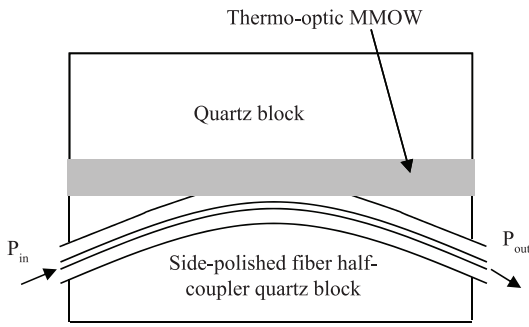


Figure 17a: Schematic diagram of the sensing device.

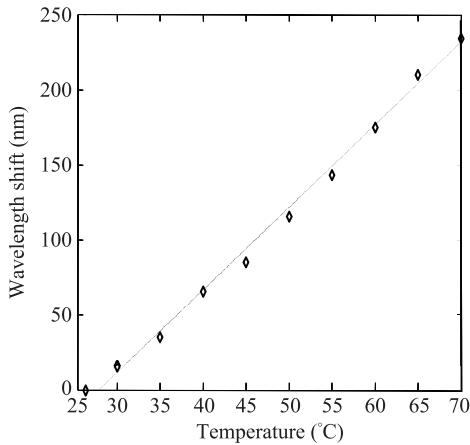


Figure 17b: Shift in the resonance wavelength with temperature; solid curve is a linear fit through experimental data points.²²

suitable MMOW material of appropriate thickness can be chosen to adapt such a device for the measurement of temperature in other ranges. Further refinement in this fiber refractometer was reported in Ref. [22], in which the role of a tapered MMOW was investigated. Such an SPF-MMOW configuration was earlier exploited as a refractometer,²³ whose performance is theoretically explained in in Ref. [24].

4 Phase Modulated FO Sensors

Interferometric fiber optic sensors with ultra-high sensitivities are based on interferometric measurements of measurand-induced change in the phase of the light propagating in a fiber.^{26–28} These sensors offer huge potential for measurements of low magnitudes. Often, their sensitivity impedes accurate measurements due to perturbations arising from ambient conditions and hence post-measurement signal processing becomes critical. Interferometer

sensitivity depends on two basic criteria: the efficiency of the interface between the measurand and the optical delay in the fiber and the ability to reject the interfering measurands at the same time.²⁷ Phase sensitivities also vary with measurands. Typical sensitivities for strain is around 10 radians per microstrain per meter, for temperature, it is about 100 radians per degree per meter, and for pressure, it is around 10 radians per bar per meter. In view of the relatively higher sensitivity to strain, pressures and magnetic fields are also measured through corresponding transformations to strain as in fiber optic hydrophones and magnetometers.²⁸ There could be a variety of FO interferometers—Mach-Zehnder, Michelson, Sagnac, and Fabry-Perot.

As shown in Figure 18a, FO version of a Mach-Zehnder Interferometric (MZI) sensor is formed by concatenating two 3-dB (50/50) couplers in the form of an interferometer.

If the amplitude of the light injected into port 1 is E_{in} , the corresponding intensity will be I_{in} ($= |E_{in}|^2$). If we consider the light from port 1 reaching port 2 via the upper and lower arms of

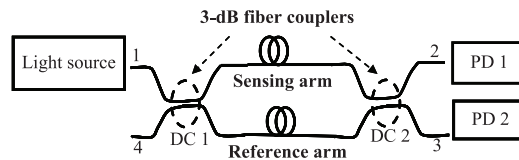


Figure 18a: A fiber optic Mach-Zehnder interferometer, in which two 3-dB fiber couplers (DC1,2) are concatenated to form it; PD1, 2 are two photodetectors, either of which could be used to record the interference pattern.

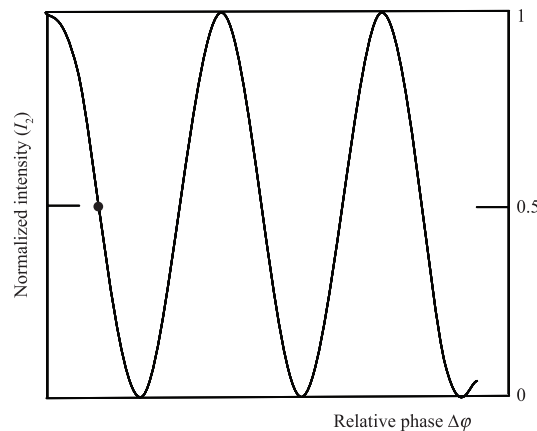


Figure 18b: Mach-Zehnder interferometer output intensity I_2 with variation in phase; the quadrature point at which $\Delta\phi$ is $\pi/2$ is represented through a 'dot' on the figure for which normalized I_2 is 0.5.

the interferometer, its intensity detected by PD₁ would be

$$I_1 = E_1 \cdot E_1^* = \frac{1}{2} E_{in} \left[e^{i\varphi_1} + e^{i(\pi + \varphi_2)} \right] \times \frac{1}{2} E_{in} \left[e^{-i\varphi_1} + e^{-i(\pi + \varphi_2)} \right] = \frac{I_{in}}{2} (1 - \cos \Delta\varphi) = I_{in} \sin^2 \frac{\Delta\varphi}{2} \quad (4)$$

where $\Delta\varphi = \varphi_1 - \varphi_2$; $\varphi_{1,2}$ correspond to respective phase accumulated along lengths of the upper and lower arms of the interferometer. In Eq. (4), an extra $\pi/2$ phase has been included which originates from the fact that phase accumulated by the crossed over light at each of the two fiber couplers²⁹ is $\pi/2$. This explains for the additional phase of π accumulated by the light traveling via the lower arm of the interferometer to reach PD₁ after crossing over twice at the two couplers. By complementarity, the intensity of light reaching PD₂ will be given by

$$I_2 = I_{in} \cos^2 \frac{\Delta\varphi}{2} \quad (5)$$

Normalized I_2 versus $\Delta\varphi$ is plotted in Figure 18b. For $\Delta\varphi = 0$, $I_2 = I_{in}$ while for $\Delta\varphi = \pi$, $I_2 = 0$.

The corresponding plot of I_1 with $\Delta\varphi$ would be complimentary to it. In practice, measurand induced $\Delta\varphi$ is small, and hence any variations in φ would be very small around the maximum and minimum of $I_{1,2}$ as a function of $\Delta\varphi$. The most sensitive point of operation would correspond to the *quadrature point*, where $\Delta\varphi = (2m + 1) \pi/2$; $m = 0, 1, 2, \dots \Rightarrow \Delta\varphi$ is $\pi/2$, or $3\pi/2$, or $5\pi/2$, \dots . Around this region, $I_{2,1}$ varies linearly with phase. This phase bias can be achieved by stretching the fiber, for example, by wrapping a section of the reference fiber arm on a piezoelectric drum driven by a signal generator; any small deviation in $\Delta\varphi$ around the quadrature bias point can be actively controlled. Thus, if the measurand induced phase change is $\delta\varphi$ around the quadrature point, $\Delta\varphi = \pi/2 + \delta\varphi$ and

$$I_1 = I_{in} \sin^2 \left(\frac{\pi}{4} + \frac{\delta\varphi}{2} \right) \approx \frac{I_{in}}{2} (1 + \delta\varphi) \quad (6)$$

It shows that $I_1 \propto \delta\varphi$, i.e. the phase difference is converted into intensity, which can be measured by a square-law detector. For a shot noise limited detection system, assuming SNR = 1, it can be shown that the minimum detectable phase change over a detection frequency bandwidth ($\Delta\nu$) is given by²⁹

$$\delta\varphi_{Min} = 2 \left(\frac{e\Delta\nu}{I_{in}\rho} \right)^{1/2} \quad (7)$$

where ρ is responsivity (amp/W) of the detector and e is the electron charge = 1.6×10^{-19} C. If $I_{in} = 1$ mW, $\Delta\nu = 1$ Hz, and $\rho = 0.5$ A/W, $\delta\varphi_{Min}$ from Eq. (7) is $\cong 3.6 \times 10^{-8}$ rad, which is indeed very small. However, since a detector is usually not shot noise limited, measurable $\delta\varphi_{Min}$ is about one to two orders of magnitude larger in practice.

If the phase of the propagating light in a fiber of length L varies due to a temperature change ΔT , then $\Delta\varphi$ can be expressed as

$$\Delta\varphi = k_0 \left(L \cdot \Delta T \frac{dn_{eff}}{dT} + n_{eff} \cdot \Delta L \right) \quad (8)$$

where dn_{eff}/dT represents the thermo-optic coefficient. Thus,

$$\frac{\Delta\varphi}{L\Delta T} = k_0 \left(\frac{dn_{eff}}{dT} + n_{eff} \frac{\Delta L}{L\Delta T} \right) \quad (9)$$

In fibers, the thermo-optic coefficient dominates over the linear expansion term, thus the first term within the bracket in Eq. (9) is the dominating term for determining the phase change per unit length of a silica fiber due to variations in temperature. It is apparent from above that the signal would vary from a maximum ($= I_{in}$) to a minimum ($= 0$) depending on $\Delta\varphi$. However, in practice this complete modulation is not observed and one can associate fringe visibility V defined through

$$V = \frac{I_{max} - I_{min}}{I_{max} + I_{min}} \quad (10)$$

so that

$$I_{2,1} = \frac{I_{in}}{2} (1 \pm V \cos \Delta\varphi) \quad (11)$$

In the early days of fiber optic MZI development, detection of acoustic waves, which led to development of fiber optic hydrophones (see Figure 19) by scientists at Naval Research Laboratory in Washington USA, was the most widely pursued sensing scheme based on fiber optic MZI.³⁰

In addition, fiber optic MZIs have been extensively used to detect temperature, linear strain,

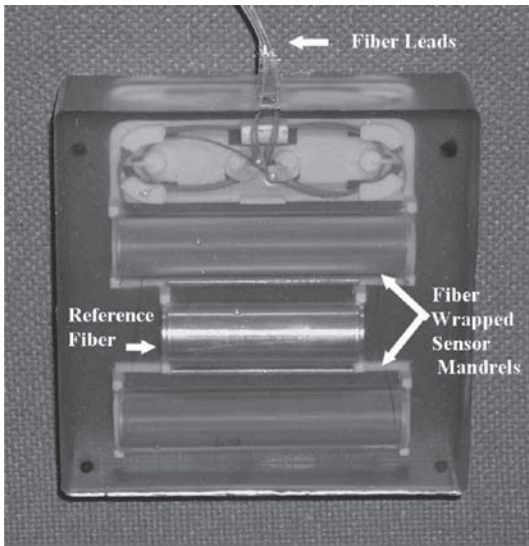


Figure 19: Photograph (courtesy J. H. Cole of NRL) of a Virginia class fiber optic hydrophone developed at the Naval Research Laboratory, Washington; adapted from (Cole *et al.* 2004) with the permission of the Washington Academy of Sciences.

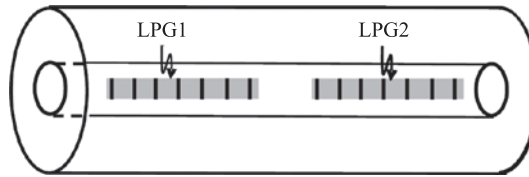


Figure 20: Schematic of a MZI formed with a pair of LPGs separated by a certain distance. LPG₁ induces partial coupling of power from the core mode to a cladding mode, which after propagating as a cladding mode re-couples back to the core mode after interacting with the second LPG. These two sets of beams taking different paths, when recombine after the second LPG form interference pattern that is characteristic of a MZI.

axial load, electric field, magnetic field, seismic signals, and vibration.²⁶ In more recent times, a pair of long period gratings (LPGs) within a fiber was shown to effectively function as a MZI^{31–33} as illustrated in Figure 20.

Since n_{eff} in the cladding is smaller than that at the core, the two different paths taken by the two distinct beams namely, a core mode and a core-cladding-core mode, lead to an optical path difference, and hence forms a two beam interference pattern similar to that in a MZI described earlier. Such LPG pair-based MZIs were shown to be capable of detecting refractive index changes as low as $\sim 1.8 \times 10^{-6}$ for hydrogen detection.³¹ Hydrogen sensing/leak detection have become extremely important in the context of fuel cells in recent times. Several other techniques have been reported for forming in-fiber MZIs including the use of photonic crystal fibers.³⁴

Fiber optic Michelson Interferometers (MI) form another platform for two beam interferometric sensors similar to MZIs, the difference being that they involve only one 3-dB fiber coupler to split one beam into two, both of which are reflected back by two mirrors placed at their ends as shown in Figure 21a.

The light from the source splits into two beams, shown in the figure as full thick arrows at the 3-dB coupler. The reflected beams reach the photo detector at port 4, where they interfere. These beams destructively interfere at Port 1 as part of

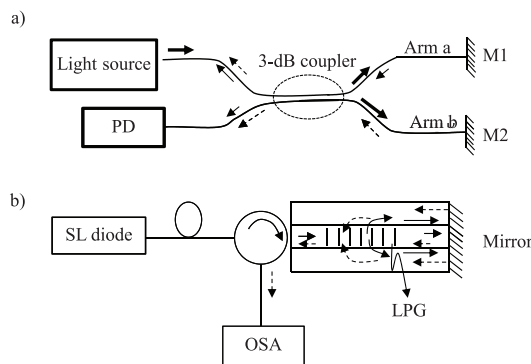


Figure 21: a) A fiber optic Michelson interferometer, in which one of the arms functions as a reference arm. The other arm as the signal arm is exposed to a measurand, which induces a change in the optical path length and hence the relative phase between the two light paths varies. As a result an interference pattern is formed at the Photo Detector (PD), which varies with the measurand; b) an alternative version of a fiber optic Michelson interferometer for sensing, in which an LPG is used to split and recombine reflected core and cladding mode lights to form interference and the same is captured on an OSA; a circulator is used in place of a fiber coupler (after Ref. [37] © IOP).

the reflected beams reaching back the source via arms 'a' and 'b' reach there with a phase difference of π . Algebraic analysis for the transmittance of a MZI presented in the previous section can be extended to analyse transmittance of a MI and it can be shown that at the port containing PD³⁵

$$I_4 = \frac{I_{\text{in}}}{2} (1 + V \cos(\Delta\phi)) \quad (12)$$

where $\Delta\phi = \phi_a - \phi_b$. Essentially, one MI is half of one MZI. Thus, all discussions made earlier for MZIs are valid here as well. The fiber coupler,

in principle, can be replaced with a circulator as shown in Figure 21b. An interesting compact version of such a single fiber-based MI without involving a fused fiber coupler was proposed in the literature,^{36,37} the basic concept of which is shown in Figure 21b.³⁷ A Long Period Grating (LPG) of about 50% coupling strength divides the propagating light in the core into two paths—one along the core via the LPG and the other along the cladding as a cladding mode—both of which are reflected by a common mirror fabricated directly at the end of the fiber. These two reflected beams form the two arms of the MI and the interference fringes after being mixed through the same LPG at the input side, which is captured through a circulator on an Optical Spectrum Analyser (OSA). Such an MI has been used as a refractometer. Cross-sensitivity to temperature is minimized in these measurements by using two different types of fibers³⁸ or a photonic crystal fiber.³⁹

Rotation sensing is of significant interest in several areas. Examples include inertial navigation systems in aircrafts/spacecrafts, in the determination of torsional oscillations in earth due to earthquakes, determination of astronomical latitude, and in monitoring polar motion due to various geophysical effects.⁴⁰ Traditionally, rotations are sensed by mechanical gyroscopes based on spinning wheels and have relied on the conservation of angular momentum. However, Fiber-based Optical Gyroscopes (FOGs) have attracted a much stronger interest in recent times due to the absence of moving parts and warm up time and sensitivity to gravity. FOGs have emerged as an offshoot of Ring Laser Gyroscopes (RLG), first reported by Rosenthal in 1962. RLGs are now routinely used for inertial navigation in many passenger aircrafts³⁴ whose navigational controls depend critically on accurate rotation sensors. Typical precision required for aircraft navigation lies in the range of 0.001–0.01°/hr. In terms of rotation rate of earth ($\Omega_E = 15^\circ/\text{hr}$), this amounts to 10^{-4} – 10^{-3} times Ω_E . The first proposal for implementing a FOG in the form of a Sagnac interferometer was made in 1976.⁴¹ These sensors are fabricated commercially to support high-end automobile navigation systems, for the pointing and tracking of satellite antennas, inertial navigation for aircrafts and missiles, and as back-up guidance system for commercial aircrafts such as Boeing 777.⁴² Other areas where fiber gyros find applications are mining, tunneling, radio-controlled attitude control of helicopters, and guidance for unmanned trucks and so on. In an FOG, two oppositely directed light beams are divided

into two counter propagating beams through a few hundreds of meter long single-mode fiber coil/loop—one in clockwise (*cw*) and the other in counter clockwise (*ccw*) direction as shown in Figure 22a.

These counter propagating *cw* and *ccw* beams exiting from the fiber loop are recombined to form the interference pattern at the photo detector (PD) for further signal processing. Two couplers, FC1 and FC2, are required to make the *cw* and *ccw* propagating beams experience identical paths, because an additional fixed phase retardation of $\pi/2$ (in the absence of measurand) is introduced by the coupler to the coupled beam. In order to understand the working principal, we outline below the simple analysis given in,⁴⁰ which ignores relativistic mechanics. Let us consider a disc of radius R that is rotating clockwise with an angular velocity Ω about an axis perpendicular to the plane of the disc as shown in Figure 22b. Two views of practical versions of robust FOGs developed by the FOG group at RCI Hyderabad are shown in Figures 22c and d.

If we assume that two identical photons are sent *cw* and *ccw* along the circumference starting at an arbitrary location 1, then, by the time *cw* propagating photon returns to its starting point, the disc would have rotated to location 2. Thus, this photon would be required to travel an extra linear distance (as compared to the case when the disc remains stationary, i.e. for $\Omega = 0$, in which case physical path length $L (= 2\pi R$, i.e. the perimeter of the disc)) of

$$L_{cw} = 2\pi R + R\Omega t_{cw} \equiv c_{cw} t_{cw} \quad (13)$$

and likewise, the *ccw* propagating photon would take a shorter path length given by,

$$L_{ccw} = 2\pi R - R\Omega t_{ccw} \equiv c_{ccw} t_{ccw} \quad (14)$$

where $R\Omega (= \Delta S)$, and $t_{cw, ccw}$ represent the times taken to cover the distances $L_{cw, ccw}$, and $c_{cw, ccw}$ correspond to velocity of light respectively. Thus, the net time difference between the two counter propagating beams to cover $L_{cw, ccw}$ is given by

$$\Delta t = \frac{2\pi R}{c_{cw} - R\Omega} - \frac{2\pi R}{c_{cw} + R\Omega} \equiv \frac{4\pi R^2}{c^2} \Omega = \frac{4A}{c^2} \Omega \quad (15)$$

where we have assumed that in vacuum light velocity $c_{cw} = c_{ccw} = c$ and the product $R^2\Omega^2$ is negligible relative to c^2 . Equivalently this time difference amounts to a path length difference of

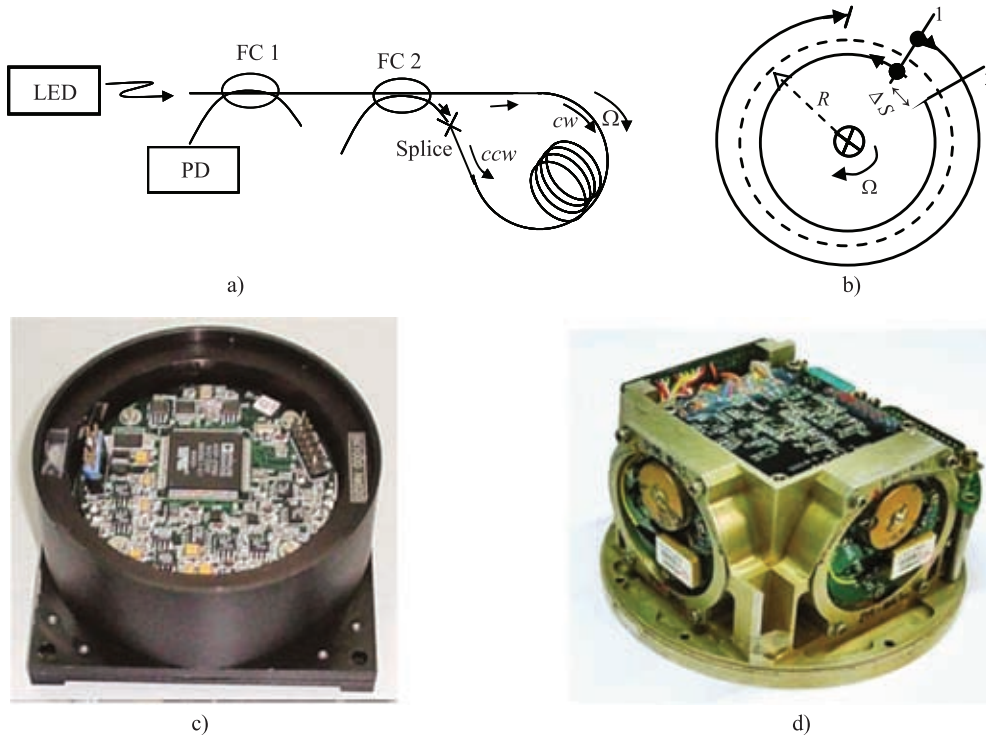


Figure 22: a) Fiber optic Sagnac interferometer for rotation sensing; FC1 and 2 represent two fiber couplers; PD is photodetector for measuring the interference between the counter propagating *cw* and *ccw* beams; Ω represents angular velocity of the rotating frame on which the fiber loop is mounted; b) Functional principle of Sagnac interferometer for rotation sensing (see text for explanation) (After Refs. [34,40]); c) Picture of a practical FOG developed by the FOG group at RCI Hyderabad d) another view of such a practical FOG [pictures courtesy Dr Jagannath Nayak].

$$\Delta L = c\Delta t = \frac{4A}{c}\Omega \quad (16)$$

Even if the Sagnac effect is considered in a medium of refractive index n , for which relativistic addition of the light velocity in that medium with the tangential velocity $R\Omega$ is required, Δt and ΔL would still be given by the Eqs. (15) and (16), respectively.⁴⁰ If that medium is a single-mode fiber wound N number of turns in the form of a coil as shown in Figure 22a then

$$\Delta t = \frac{4AN}{c^2}\Omega \Rightarrow \Delta L = c\Delta t = \frac{4AN}{c}\Omega \quad (17)$$

The phase difference $\Delta\phi$ between the *cw* and *ccw* propagating beams would be given by

$$\begin{aligned} \Delta\phi = k_0 c \Delta t &= \frac{8\pi AN}{\lambda_0 c} \Omega \Rightarrow \Delta L = \frac{\Delta\phi}{k_0} \\ &= \frac{4AN}{c} \Omega = \frac{LD}{c} \Omega \end{aligned} \quad (18)$$

where D is diameter of the fiber, and $N = L/(\pi D)$. The output intensity from a Sagnac interferometer

due to interference between the *cw* and *ccw* propagating beams can be shown by following the analysis identical to the one described for MZIs, as

$$I = \frac{I_{\text{in}}}{2}(1 + \cos\Delta\phi) \quad (19)$$

Following the same arguments as in the case of MZI before, the interferometer may be biased through use of a PZT phase modulator at the quadrature point ($\Rightarrow \Delta\phi = \pi/2 + \delta$) so that Eq. (19) becomes

$$I_{\text{out}} = \frac{I_{\text{in}}}{2}(1 - \sin\delta) \approx \frac{I_{\text{in}}}{2}(1 - \delta) \quad (20)$$

since δ in general would be small. If we assume shot-noise limited detector as in the case of MZI described above [see Eq. (3.4)], then minimum measurable Ω would be given by²⁹

$$\Omega_{\text{min}} = \frac{c\lambda_0}{4\pi AN} \left(\frac{e\Delta\nu}{\rho I_{\text{in}}} \right)^{1/2} \quad (21)$$

If we assume a fiber length of 500 m spooled in a loop of 3.2 cm radius, $\rho = 0.5$ A/W, $I_{in} = 1$ mW, $\lambda_0 = 1.3$ μm , and $\Delta\nu = 1$ Hz, then $\Omega_{min} \sim 30 \times 10^{-8}$ rad/s. Several companies market application-specific FOGs, e.g. for missile guidance systems, commercial aircraft navigation systems, military helicopters as well as marine and submarine navigation systems, gas pipe mapping, compasses for tunnel construction, rockets, and even for automotive navigation systems.³⁴ Birefringent fibers (including birefringent microstructured fibers) have been also used in fiber optic Sagnac interferometers for measurement of pressure,⁴³ temperature,⁴⁴ strain, and temperature,⁴⁵ multiple beam Sagnac topology,⁴⁶ twist sensor,⁴⁷ cladding-mode resonance-based Sagnac Interferometer⁴⁸ and curvature.⁴⁹

In all the above sensors, the interaction of the measurand with the guided light in a fiber is most important and the same needs to be maximized for maximum sensitivity of the sensor. In order to enhance this interaction, and hence the sensitivity, one can design the sensor in such a way that the light is made to traverse the same length of the signal fiber several times, which is possible through use of multiple beam interferometry like that in a Fabry-Perot Interferometer (FPI). In general, an FPI, often referred as an FP etalon, is composed of two parallel reflecting surfaces with a small separation between them as shown in Figure 23a.

In intrinsic fiber form (referred to as FFPI in the literature), the reflecting mirrors are either within the fiber itself as shown in Figure 23b by forming Bragg gratings,^{52,53} or through micromachining,^{54,55}

chemical etching,⁵⁶ or by coating the cleaved end of the fiber with titanium dioxide and re-splicing with a section of identical fiber.⁴² On the other hand, an extrinsic version (referred to as EFPI) is shown in Fig. 23c, in which one mirrored end of each fiber forms the two reflectors with an air gap in between; portions of the two mirrored fiber ends are kept inside a capillary for mechanical stability. In both cases, R1 and R2 together with a separation in between form a cavity of length L ; light entering the cavity through partially reflecting R1 is partially reflected and partially transmitted through R2. The reflected wave from R2 undergoes further partial reflections at R1 and R2. Those wavelengths for which L is an integral multiple of half the wavelength within the cavity (resulting one round trip through the cavity is an integral multiple of the wavelength), would add in phase on transmission through R2. Any perturbation to the cavity in terms of its length or refractive index by a measurand through either of the mirrors would affect the optical path length of the cavity. In principle, the cavity could be extremely small mimicking a point sensor. It may be noted that a fiber optic FPI sensor is less complex than fiber optic MZI and MI sensors described earlier as the FPI sensor does not require any couplers. The earliest fiber optic FPI sensors used well cleaved fiber end faces⁵⁷ or dielectric mirrors as the mirrors.^{58,59} If we neglect any potential loss due to scattering and absorption in the mirrors, classical expressions for transmittance, defined as the ratio of transmitted power to incident power and likewise for reflectance of the mirrors in a FPI are given by⁶⁰

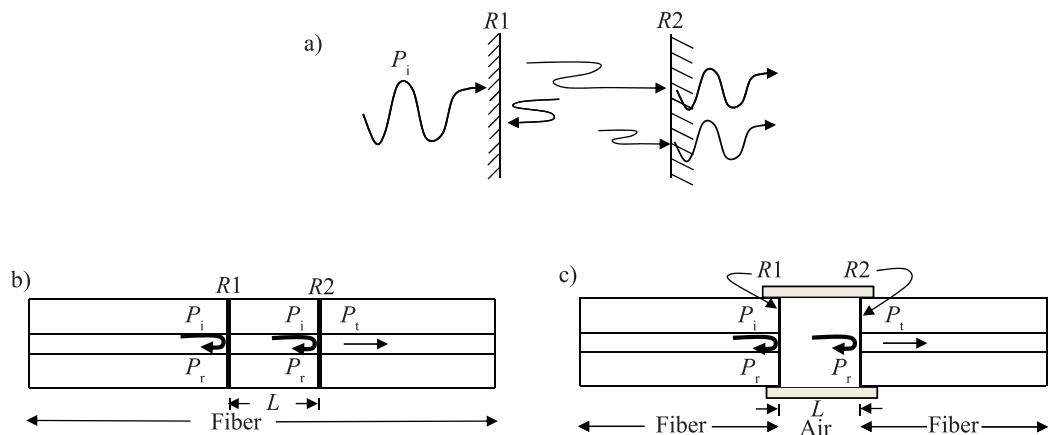


Figure 23: a) Basic structure of Fabry Perot Interferometer (FPI); input power P_i is incident on a mirror having reflectivity $R1$. Part of this light is transmitted and partly reflected by the mirror, while the transmitted light gets again partially reflected and transmitted at the mirror $R2$. b) Intrinsic and c) extrinsic FPI-based fiber optic sensor (after Refs. [50,51]).

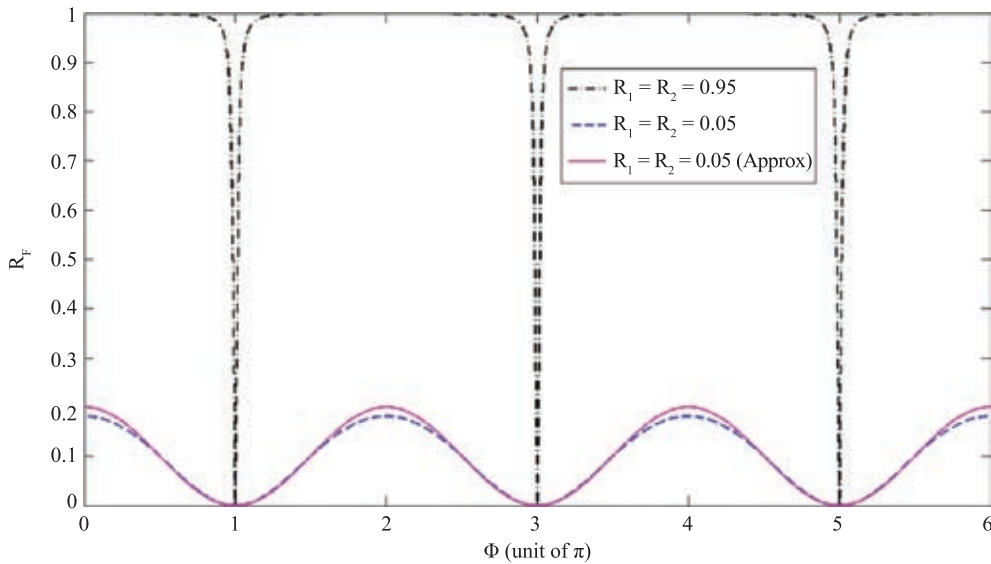


Figure 24: FPI reflectance as a function of phase Φ as determined by Eq. (23) for $R = 0.95$ and $R = 0.05$. For the latter case of low mirror reflectivity the full curve is obtained from the approximate relation Eq. (26), indicating it is indeed a valid expression (Figure courtesy Ajanta Barh).

$$T_{\text{FP}} = \frac{T_1 T_2}{1 + R_1 R_2 + 2\sqrt{R_1 R_2} \cos \phi} \quad (22)$$

$$R_{\text{FP}} = \frac{R_1 + R_2 + 2\sqrt{R_1 R_2} \cos \phi}{1 + R_1 R_2 + 2\sqrt{R_1 R_2} \cos \phi} \quad (23)$$

where ϕ the round-trip propagation phase shift through the cavity having a refractive index n , and length L , is given by

$$\phi = \frac{4\pi n L}{\lambda_0} \quad (24)$$

Naturally, T_{FP} is maximum for $\phi = (2p + 1)\pi$ with $p =$ an integer. The Eqns. (22) and (23) are valid for fiber optic FPIs also. In particular, for fiber FPIs (FFPIs) having low reflectance and by assuming $R_1 = R_2 = R$ ($\ll 1$), these equations simplify to⁵⁰

$$T_{\text{FFP}} \cong 1 - 2R(1 + \cos \phi) \quad (25)$$

$$R_{\text{FFP}} \cong 2R(1 + \cos \phi) \quad (26)$$

Equations (25) and (26) are plotted in Figure 24 as a function of round trip phase ϕ . In order to test the validity of the approximate expression Eq. (26) for low mirror reflectivity, R as a function of ϕ is shown in the same figure as a full curve.

FFPI sensors provide high sensitivity, large dynamic range, and fast response for measurement

of pressure, temperature, strain, displacement, magnetic field, flow rate, etc. and can also be used as embedded sensors in materials.^{50,51} Detection of acoustic noise bursts produced by breaking a pencil lead on the surface of an aluminum sample by an EFPI has also been demonstrated as a pressure sensor.⁶¹ Other FFPI sensors have been reported for measurement of humidity,⁶² displacement,^{63,64} and magnetic fields.⁶⁵

5 Wavelength Modulated FO Sensors

In-fiber gratings are extensively used in dense wavelength division multiplexed optical communication links, and are also attractive as strain and temperature sensors, in particular for distributed measurements.⁶⁶ An important attribute of fiber grating sensors over typical fiber optic intensity modulated sensors is that the measurement and information is wavelength-encoded, which makes the sensor self-referencing, i.e., independent of fluctuations in source intensity during a measurement.^{67,68}

A schematic of a Fiber Bragg Grating (FBG) of spatial period Λ , which is written interferometrically inside the photosensitive Germania-doped silica core-silica clad single-mode fiber is shown in Figure 25. Two obliquely incident UV beams are made to interfere leading to a periodic variation in refractive index in the photosensitive core region exposed to the interference pattern.

When light from a broadband source propagates in an FBG, a specific wavelength referred to as the Bragg wavelength (λ_B) within the bandwidth

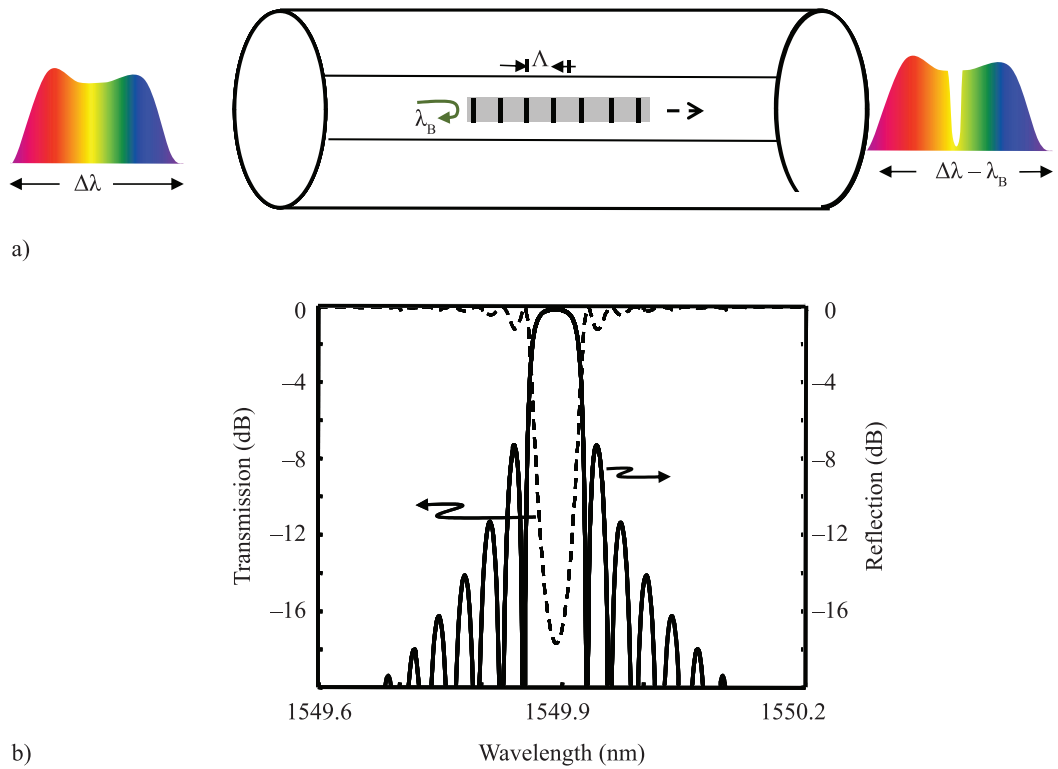


Figure 25: a) Schematic of a Fiber Bragg Grating (FBG) inside the core which is wavelength encoded with a specific Bragg wavelength λ_B , which gets reflected out of a broad band light launched into the fiber, rest of the spectrum is transmitted; b) typical reflection and transmission spectra of a FBG (Figure courtesy Parama Pal).

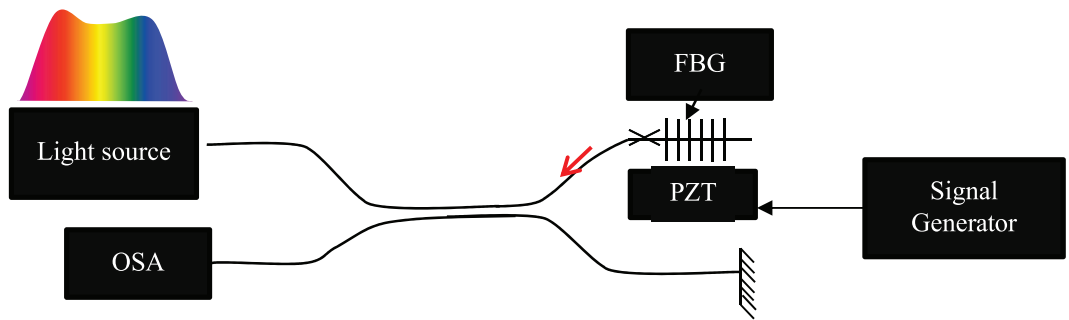


Figure 26: A fiber optic Michelson interferometer containing a FBG spliced to one of its arms, which is mounted on a PZ ceramic resonator driven by a signal generator, which could induce stretching of the FBG containing arm. One of the wavelengths (λ_B) from a broadband light source is reflected by the FBG. The reflected signal in both strained and unstrained cases are detected and measured in an Optical Spectrum Analyzer (OSA) placed at the second input port.

of the source that satisfies the following phase matching Bragg condition:

$$\lambda_B = 2n_{\text{eff}} \Lambda \tag{27}$$

undergoes strong reflection while the rest of the spectrum gets transmitted; here n_{eff} represents the fiber mode effective index. This is depicted

in Figure 26b. Due to the wavelength-encoded response (of the reflected light), several fiber gratings of different spatial periods formed at different locations on the same fiber enable distributed measurements of strain and temperature. This feature is very attractive for local damage detection in civil structures like bridges, buildings,⁶⁹ and also aircrafts,^{70,71} etc., as well as for internal

strain mapping with high spatial resolution.⁶⁸ The characteristic optical path length η in a fiber grating is given by the product of n_{eff} with spatial wavelength (Λ) of the grating. The parameter η would depend on both stress (σ) and temperature (T), and hence, a change $\Delta\eta$ in η with respect to a reference value is given by⁷²

$$\begin{aligned}\Delta\eta(\Delta\sigma, \Delta T) &= \eta(\sigma, T) - \eta(\sigma_r, T_r) \\ &= \left[\frac{\partial\eta}{\partial\sigma} \right]_{T_r} \Delta\sigma + \left[\frac{\partial\eta}{\partial T} \right]_{\sigma} \Delta T\end{aligned}\quad (28)$$

where the subscript 'r' refers to reference value, while $\Delta\sigma$ and ΔT represent incremental changes in the local stress and temperature from their reference values. For an FBG, it is known that peak reflection at the Bragg wavelength (λ_B) is given by²⁸

$$R_{\text{peak}} = \tanh^2(\kappa L)\quad (29)$$

Thus Eq. (28) can be rewritten as

$$\begin{aligned}\frac{\Delta\lambda_B}{\lambda_B} &= \left[\left[\frac{\varepsilon}{\partial\sigma} \right]_{T_r} + \frac{1}{n_{\text{eff}}} \left(\frac{\partial n_{\text{eff}}}{\varepsilon} \right)_{T_r} \left(\frac{\varepsilon}{\partial\sigma} \right)_{T_r} \right] \Delta\sigma \\ &+ \left[\left(\frac{\varepsilon}{\partial T} \right) + \frac{1}{n_{\text{eff}}} \left(\frac{\partial n_{\text{eff}}}{\partial T} \right)_{\sigma} \right] \Delta T\end{aligned}\quad (30)$$

where the strain, denoted by ε , is given by

$$\varepsilon = \pm \frac{\partial\Lambda}{\Lambda}\quad (31)$$

The \pm signs represent tensile and compressive stress, respectively. In terms of Young's modulus (Y_F) and thermal expansion coefficient (α_F), Eq. (30) can thus be rewritten as

$$\begin{aligned}\frac{\Delta\lambda_B}{\lambda_B} &= \frac{1}{Y_F} \left[1 + \frac{1}{n_{\text{eff}}} \left(\frac{\partial n_{\text{eff}}}{\varepsilon} \right)_{T_r} \right] \Delta\sigma \\ &+ \left[\alpha_F + \frac{1}{n_{\text{eff}}} \left(\frac{\partial n_{\text{eff}}}{\partial T} \right)_{\sigma} \right] \Delta T \\ &= \left[1 - \frac{n_{\text{eff}}^2}{2} p_e \right] \varepsilon_z + \left[\alpha_F + \frac{1}{n_{\text{eff}}} \left(\frac{\partial n_{\text{eff}}}{\partial T} \right)_{\sigma} \right] \Delta T \\ &= S_{\varepsilon} \Delta\sigma + S_T \Delta T\end{aligned}\quad (32)$$

where ε_z is the strain along fiber axis, and p_e represents an effective strain-optic or photo-elastic coefficient defined through

$$p_e = [p_{12} - \nu(p_{11} + p_{12})]\quad (33)$$

Here p_{11} and p_{12} are Pockel's (piezo) coefficients, i.e., components of the strain optic tensor, ν is Poisson's ratio, while S_{ε} and S_T represent strain and temperature sensitivities, respectively. For a typical germano-silicate fiber, values of p_{11} , p_{12} , and ν are 0.113, 0.252, and 0.16 respectively. With n_{eff} equal to 1.482 at 1550 nm, the strain sensitivity at this wavelength region is 1.2 pm/ $\mu\varepsilon$ ³⁴ and shift in Bragg wavelength is typically almost linear with strain (ε). The mirror characteristic of FBGs opens new possibilities for interferometric sensing. As an example, a fiber optic Michelson interferometer based on a fiber coupler, in which a FBG is placed in one of its arms, as shown in Figure 26, is used to measure strain-induced shifts in its Bragg wavelength.

Figure 27 depicts sample results from measurements of small strains using FBGs fabricated by the Fiber Optics Group at the Central Glass and Research Institute (CGCRI, Kolkata, India), where the sensitivity was 1.215 pm/ $\mu\varepsilon$.^{73,74}

Results reported on fiber grating sensors indicate their capability to measure dynamic strain from DC to over 10 MHz with strain resolutions of 0.02 $\mu\varepsilon$ (DC to 10 KHz) to 25 $\mu\varepsilon$ (10 MHz). Many bridges and other civil structures around the world are now retro-fitted with FBGs as strain gauges for distributed measurements of strain. Large arrays of FBG strain sensors, each of which is uniquely wavelength encoded in term of individual λ_B , can be sequentially interrogated by a broadband source as shown in Figure 28. Different topologies for multiplexing of fiber optic sensors have been discussed in detail in Ref. [75].

FBGs are also used to detect ultrasound propagating in structures and for monitoring both static and dynamic strain fields.⁷⁶ Experiments have indicated that dynamic strains up to 10^{-2} $\mu\varepsilon$ or smaller and frequencies ~ 1 MHz are detectable by FBGs.⁷⁷ When cracks develop in a civil structure due to fatigue and loading, bursts of ultrasonic waves are generated that propagate through the structure. By detecting this acoustic emission (which occurs due to transient elastic waves within a material caused by the release of local stress energy), alarms can be triggered for signalling structural failure.

If we consider temperature sensitivity S_T [Eq. (32)], the first term α_F representing thermal expansion coefficient of the fiber, which for silica is $\sim 0.55 \times 10^{-6}/^\circ\text{C}$, whereas the second term namely, the thermo-optic coefficient term is $\sim 8.6 \times 10^{-6}/^\circ\text{C}$, which is naturally the more dominating term. At $\lambda_B = 1550$ nm, change $\Delta\lambda_B \sim 0.013$ nm/ $^\circ\text{C}$. Temperature change strongly impacts FBG signals, and hence it is important to realize that precise strain measurements

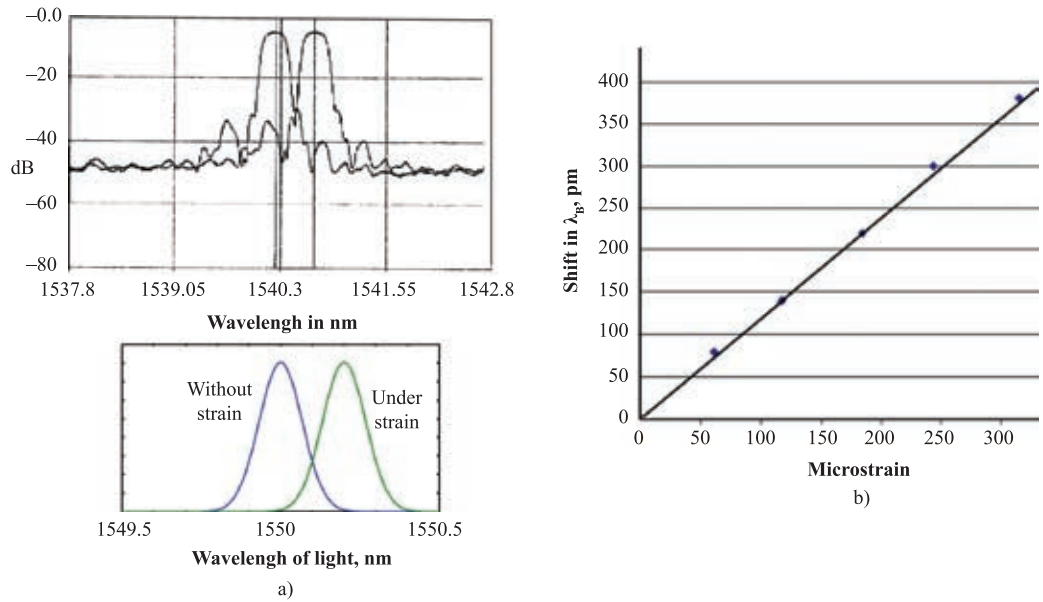


Figure 27: a) Optical spectrum analyzer trace of reflected light from a fiber Bragg grating showing shift of the reflection spectrum due to strain and corresponding shift in the Bragg wavelength; b) measured shift in Bragg wavelength as a function of strain ($\mu\epsilon$). These measurements were carried out in the Fiber Optics Laboratory at CGCRI (Kolkata) [Figures courtesy T. K. Gangopadhyay].

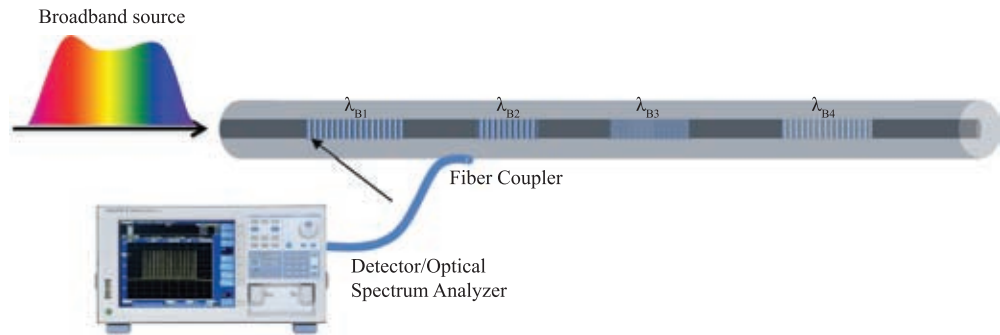


Figure 28: Distributed strain measurement with an array of FBGs of different pitch attached/embedded in e.g. a civil structure or an aircraft or a ship for monitoring its health (Figure courtesy Parama Pal).

require proper temperature compensation. Since fractional change in λ_B depends on both strain and temperature, it is important to note that for absolute measurements of either of these parameters, one needs to de-convolve the second effect. An additional FBG could be deployed in parallel, which is isolated from the measurand and through appropriate calculation measurand signal could be corrected. Figure 29a depicts sample results on temperature measurements with in-house fabricated FBG carried out by the Fiber Optics Group at CGCRI (Kolkata); λ_B at room temperature of this FBG was 1545 nm. CGCRI group, in collaboration with SINTEF (Trondheim, Norway), had successfully installed FBGs to monitor real-time local temperature directly in real world 400 KV electric power transmission lines of Power Grid

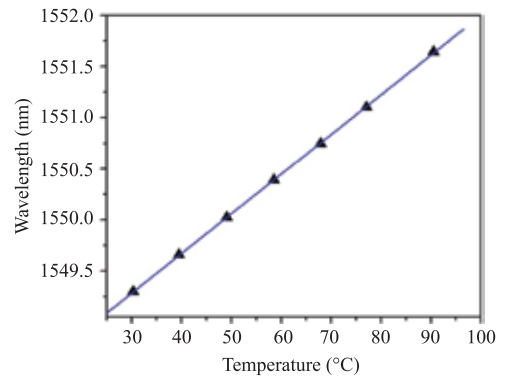


Figure 29a: Measured Bragg wavelength as a function of temperature of a FBG having Bragg wavelength of 1545 nm at room temperature.

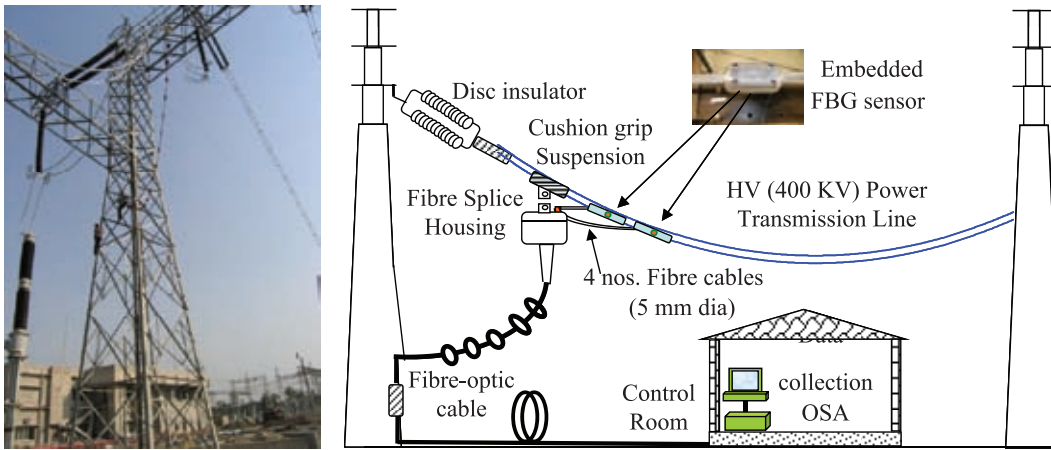


Figure 29b: Schematic layout of the field experiment carried out for real-time monitoring of temperature with a pair of FBGs in a real-world 400 KV electric power transmission lines between power transmission towers [Figures courtesy T. K. Gangopadhyay of CGCRI].

Corporation (India) at a location near Kolkata,⁷⁴ Figure 29b is a depiction of the experimental layout used for these measurements at that site.^{74,78}

Long Period Gratings (LPG) could also be used as fiber optic sensor.⁷⁹ In Ref. [80] the authors have demonstrated LPG-based sensors written on standard telecommunication fibers with temperature, strain, and refractive-index resolutions of 0.65°C, 65.8 μE , and 7.7×10^{-5} , respectively. The characteristic period Λ_{LPG} of such in-fiber gratings are typically few hundreds of μm in contrast to sub- μm period in FBGs. The transmission spectrum of the LPG exhibits a bandstop kind of filter characteristics as the LPG induces coupling of power from the core mode LP_{01} to cladding modes. In contrast to Eq. (27) the corresponding phase matching equation for a LPG leads to

$$\lambda_c = \Lambda_c (n_{e1} - n_{e2}) \quad (34)$$

where λ_c is the center wavelength at which the power coupling takes place, while $n_{e1,e2}$ represent mode effective indices of the core mode and the cladding mode involved in this power coupling process at this wavelength. Essentially the LPG acts like a filter.^{28,29} The cladding modes interact with the surrounding environment as they are formed through total internal reflection at the cladding-air interface (see Figure 30), and hence any change in the ambient properties of the surrounding medium could be detected in terms of the transmittance of the LPG and measured.

For a broadband light source, due to coupling of power from a guided to several of the cladding modes having little difference in their propagation constants, leaves a series of loss bands or

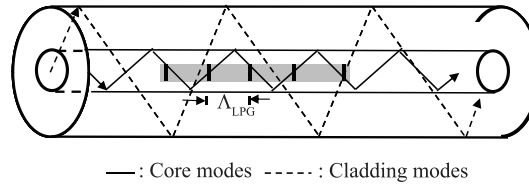


Figure 30: Schematic of a Long Period Grating (LPG) which induces power coupling from the core to the cladding modes at the phase matching wavelength λ_c given by Eq. (11); core and cladding modes are represented schematically through ray diagrams showing core and cladding modes as being formed respectively through total internal reflections at the core-cladding interface and at the cladding-air interface.

resonance dips in transmission spectrum of a LPG. Measurand-induced shift in these loss bands caused by the modified cladding mode spectrum could be exploited to get a measure of the measurand. Readers may find more details about use of in-fiber LPG as sensors in Ref. [81].

6 Polarization Modulated FO Sensors

The monitoring of electric currents in power stations is a critical requirement for reliability and stability, since sudden surges need to be detected so that the failed section can be isolated from the power system network to minimize damage and system failure. Current Transformers (CTs) are most often used as current sensors in power protection relay systems.⁸² In a CT, an iron core and suitable wire windings are used as secondary transformer to step down the high current flowing in the primary to a much lower current (typically 1 Amp ~5 Amp). Unfortunately these devices

are subject to electromagnetic interferences, and can suffer distortions due to saturation effects and residual fields in the magnetic cores, besides being susceptible to insulation failure due to large currents (~kilo amp) in the system.³⁴ **Due to these factors, optical sensors have assumed considerable importance in recent years.**⁸² With typical transmission voltages hovering around 400 kV requiring control and switching of currents ~ few kAmps, dielectric optical fibers have become very attractive for use in communications and sensing in the power industry.⁸³ The basic concept behind optical detection of electrical current is the classical Faraday Effect.^{83,84} Faraday effect states that if a beam of plane polarized light is passed through a transparent solid or liquid is placed in a uniform magnetic field in a direction parallel to the magnetic lines of force (e.g. through the holes in the pole shoes of a strong electromagnet), its plane of polarization gets rotated (though remains plane polarized) by an angle proportional to the magnetic field intensity. The modes of light propagating in the presence of a longitudinal magnetic field are right and left circularly polarized light waves, each of which propagates with different velocities. Silica fibers exhibit the Faraday effect. When a single turn of a single-mode optical fiber encloses a current carrying conductor, the magnetic field generated around it due to the current influences the State Of Polarization (SOP) of the light propagating through the fiber through Faraday effect. The Faraday rotation of the SOP is given by

$$\theta = V \oint \vec{H} \cdot d\vec{l} \quad (35)$$

where \vec{H} is the applied magnetic field intensity, \vec{l} the length of the medium, and V is the Verdet constant of silica, which is $\cong 2.64 \times 10^{-4}$ deg/Amp

(= 4.6×10^{-6} rad/Amp). If there are N turns of fiber in the loop that surround the current carrying conductor, then by Ampere's law

$$\oint \vec{H} \cdot d\vec{l} = NI \quad (36)$$

By combining Eqs. (35) and (36), we get

$$\theta = V \cdot N \cdot I \quad (37)$$

where I is the current enclosed by a single fiber turn in the loop. Faraday rotation depends only on the magnitude of the electric current regardless of the shape or size of the loop and position of the conductor within the loop.³⁴ A schematic of the Faraday effect based fiber optic electric current sensor is shown in Figure 31.

Light from a polarized laser is passed through a half wave plate and focused onto a single-mode fiber. The fiber is wound around a current carrying conductor. Output light from the fiber is passed through a Wollaston prism or a polarization beam splitter, which divides the Faraday rotated light into two mutually orthogonal linearly polarized components, which are then detected by two independent photo detectors PD1 and PD2. The difference between the two photo detector output intensities, $I_{1,2}$, is normalized with respect to their sum, which is proportional to θ (Lee *et al.* 2006) i.e., for small θ the ratio R is³⁴

$$R = \frac{I_1 - I_2}{I_1 + I_2} = \sin 2\theta \approx 2\theta \quad (38)$$

This procedure also makes the output independent of any laser power fluctuations or drift during the measurement. In real world systems, some random birefringence could also be present;

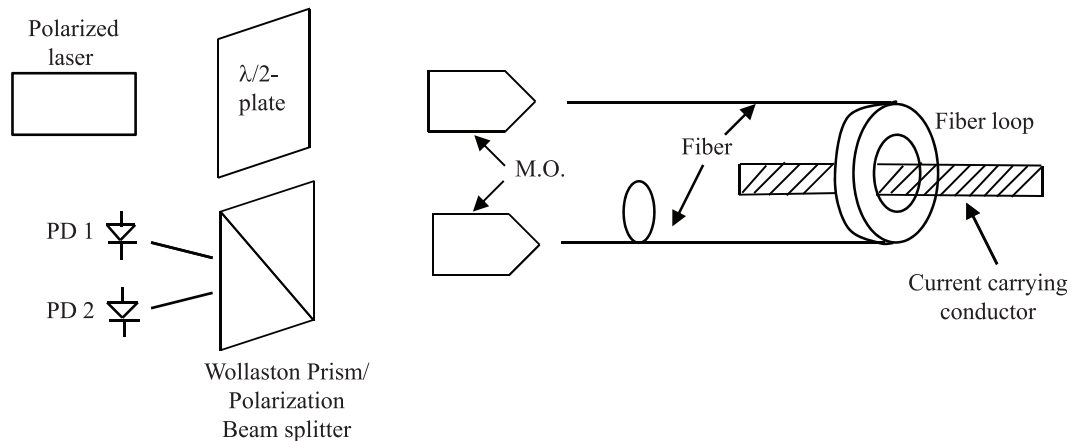


Figure 31: Schematic of fiber optic Faraday sensor for measurement of large electric current; M.O. stands for microscope objective. Functional principle is described in the text.

besides there could be bend-induced linear birefringence also present in the fiber loop especially in case of small loop radii. In the presence of linear as well circular birefringence, R is given by²⁹

$$R = 2\theta \left(\frac{\sin \Delta}{\Delta} \right) \quad (39)$$

where

$$\Delta^2 = 4\theta^2 + \delta^2; \quad \delta = k_0 \Delta n_{\text{eff}} 2\pi R_1 N \quad (40)$$

with θ in radians; Δn_{eff} is the linear birefringence, and R_1 is the fiber loop radius. Linear birefringence Δn_{eff} is inversely proportional to square of R_1 and directly proportional to square of fiber cladding radius. For the case, in which circular birefringence due to Faraday Effect dominates over linear birefringence, R is given by Eq. (39) whereas if linear birefringence dominates over circular birefringence then

$$R \approx 2\theta \frac{\sin \delta}{\delta} \quad (41)$$

In the latter case, the sensitivity is rather low.²⁹ Linear birefringence can be significantly reduced or compensated by introduction of additional circular birefringence through twists in the fiber.⁸⁵ Fiber optic Faraday current sensors have been successfully used to measure large currents (of the order of a few kilo-amperes). Faraday rotations can be also measured through fiber optic Sagnac interferometers.⁸⁶

7 FO Sensors for Biomedical Applications†

Fiber optics has gained in versatility and functionality over the past few decades and has shown significant applicability in biomedical applications, both in the laboratory as well as in clinical settings. Optical fibers are used primarily as a conduit, for the remote delivery of light and the collection of scattered and/or fluorescently emitted signals (from the tissue/sample of interest) for applications in minimally invasive diagnostics as well as therapeutic monitoring. Additionally, advances in fabrication techniques have led to fiber designs and fabrication optimized for transmissions ranging from 200 nm (for UV resonance Raman spectroscopy studies) upto nearly

3000 nm (for IR Raman spectroscopy as well as laser ablation therapies).^{87–89} The size and flexibility of optical fibers enable access to cavities and hollow tracts and can be readily inserted into solid organs, akin to a needle. Fiber sensors can also be placed non-invasively against epithelial as well as surgically exposed surfaces. In addition, the materials used in the fabrication of most optical fibers are, as mentioned earlier in this article, chemically inert and non-toxic, thus rendering them as ideal biocompatible candidates for biological sensing applications. A ‘direct’ clinical FO sensor, or a photometric sensor, is one wherein the intrinsic optical properties of the analyte or sample of interest (such as backscattered light or autofluorescence/Raman signals remitted directly from the sample), are measured. Indirect (or indicator-based) sensors, on the other hand, involve an intermediary, such as tags, labels or any other bioprobe with optically detectable characteristics (such as color change, fluorescence) for measuring the parameter of interest.⁹⁰ Biosensing (for glucose or pH measurements) is done via spectroscopic or fluorometric measurements using fibers that have appropriate molecular reagents immobilized at their ends.

White light spectroscopy, Raman spectroscopy, optical coherence tomography and fluorescence based measurements are some commonly used biomedical sensing modalities for diagnosis, oximetry, dosimetry and drug concentration evaluations. The measurement parameters for these modalities typically include absolute light intensities, scattering and absorption characteristics, and birefringence and all of these techniques can be differentiated on the ranges of sampled areas (or volumes) achieved, the cost of instrumentation and deployment, specificities and data processing complexities. A vast body of literature has been dedicated to the use of optical fibers in biomedical instrumentation and sensing and a detailed description is beyond the scope of this article. For a concise description of various sensing modalities that use optical fiber technology extensively, the reader is referred to Ref. [91].

Important considerations for choosing an appropriate FO biomedical sensor include aspects such as spatial resolution, sampling volume and the extent of invasiveness that can be tolerated along with the signal processing, and analyses of algorithms are required for the specific application. Biomedical fiber sensors are often deployed in the form of catheters and probes with the smallest dimensions that can be achieved. Flexible catheters with overall outer diameters as low as less than 0.5 mm have been previously reported.⁹² A large

†This section has been kindly contributed by Parama Pal of Robert Bosch Center for Cyber Physical Systems, IISc Bangalore.

number of research papers and scientific reports have been dedicated to probe designs (often referred to as optrode as mentioned earlier in the article) and characterizations for sensing modalities such as reflectance (both diffuse and polarized), spectroscopic, fluorescence and Raman. Probe dimensions and geometries are engineered for specific applications, whether it is imaging-based or for therapeutic (such as laser ablation therapy or thermal therapy) purpose. For instance, by altering the distal tip of the probe fiber, the path of the light entering or exiting the fiber can be redirected (to increase fluence rates for instance) and numerical apertures can be optimized so as to improve coupling efficiencies with other optical components.⁹¹ Typical fiber tip modifications include sculpting ball lenses at the end of the fiber, which are basically hemispherical-shaped ends that adjust spot sizes and beam divergences, and essentially act as focusing lenses, as well as tapering, wherein the cross-sectional dimensions of the fiber vary along its length. These end modifications are usually done by heating the fiber to a high temperature and using either gravity or tensioning (for fabricating tapers) or surface tension (for fabricating ball lenses). Raman sensing, based on the Raman effect, which is an inelastic scattering process wherein the incident photon of a certain energy (and hence, frequency) gets scattered to a lower energy (lower frequency) by a molecule as the molecule makes a transition to a vibrational state, employs flexible fiber bundles where a single fiber (typically the central fiber of the closely packed bundle) delivers the illumination and the surrounding fibers detect the light remitted from the sample. Hexagonal packing arrangements are typically the most optimal for packing into a circular cross-section. If m denotes the number of rings around the central fiber, then the maximum number of fibers that can be packed hexagonally (N_{fiber}) is given by⁹³

$$N_{\text{fiber}} = 1 + \sum_{k=0}^m 6k \quad (42)$$

Efficient fiber bundle designs have to take into careful consideration factors such as total optically active area, exit surfaces (e.g. flat vs. beveled) for the probe bundles and material choices for biosafety compliance. Optical Coherence Tomography (OCT) is a high-resolution, cross-sectional imaging modality based on low coherence interferometry which is capable of producing depth-resolved images that are derived from optical scattering arising from internal tissue microstructures.⁹⁴ Fiber endoscopes with ball lenses at the tips are often used in OCT catheters.⁹⁵

Fiber optics offer unique sensing capabilities for a diverse range of biomedical applications such as diagnosis, therapy and treatment assessment and monitoring. It has proven to be a safe, effective, affordable, and easy to use platform with significant potential for further miniaturization and expanded sensing capabilities that incorporate multiple sensing modalities into a single instrument.

8 Conclusions

This article attempts to present a unified description of the basic functional principles and applications of a variety of optical fiber sensor platforms based on intensity, phase, wavelength, and polarization modulation of light. The focus has been to explain the physics behind these sensing schemes and describe applications wherever feasible/achievable with reference to already reported results. The field of FO sensors is a subject in itself and new varieties like distributed measurements based on Brillouin scatter effect and exploitation of surface plasmon resonance-based FO sensors are lately attracting lot of attentions from researchers. Even though functional principles are rather well known, challenge lies in industrialization of these FO sensors.⁹⁶

Acknowledgement

I wish to acknowledge substantial contributions made by Dr. Parama Pal of Robert Bosch Center for Cyber Physical Systems @ IISc Bangalore in terms of editorial modifications, critical read, useful suggestions, and pointing to several biomedical applications of FO sensors. I also acknowledge with thanks some practical results on Bragg fiber-based sensors given to me by Dr. Tarun Gangopadhyay of CGCRI Kolkata. I thank Dr. Jagannath Nayak, Group Leader of FOG group at RCI Hyderabad and my former graduate student Dr. Prerana (now at RCI) for the two photographs in Figure 22. Thanks are due to Prof. S. Asokan of IISc for his kind invite to contribute this article for the special issue of the Journal of IISc on Fiber Optic Sensors and Applications. I am grateful to him for his patience as I could not meet a couple of times his deadline set for submission of the manuscript.

Received 31 July 2014.

References

1. B. P. Pal, Chapter on Optical Fiber Sensors and Devices in *Fundamentals of Fiber Optics in Telecommunication and Sensor Systems*, ed. B. P. Pal, John Wiley, New York and Wiley Eastern, New Delhi, 1992; paperback reprint editions by New Age Publishers, New Delhi, 1994, 1997, 2000, 2005, 2007, 2010, 2012, 2014.

2. F. P. Kapron, D. B. Keck, R. D. Maurer, *App. Phys. Lett.* **1970**, 17, 423.
3. B. Culshaw, Chapter on Principles of Optical Fiber Sensors in *Guided Wave Optical Components and Devices: Basics, Technology, and Applications*, ed. B. P. Pal, Academic Press/Elsevier, Burlington, MA, **2006**.
4. R. S. Medlock, Chapter on Fiber optic intensity modulated sensors in *Optical Fiber Sensors*, eds S. Martelucci and A. M. V. Scheggi, Martinus Nijhoff, Dedrecht, The Netherlands, **1987**.
5. D. A. Krohn, *Fiber Optic Sensors: Fundamentals and Applications*, Instrument Society of America, research Triangle Park, NC, **1988**.
6. B. P. Pal, Chapter on Intensity modulated fiber optic sensors in *Fundamentals of Fiber Optics in Telecommunication and Sensor Systems*, ed. B. P. Pal, John Wiley, New York and Wiley Eastern, New Delhi, **1992**; latest reprint by New Age Publishers, New Delhi, **2014**.
7. G. D. Pitt, P. Exrance, R. C. Neat, D. N. Bachelder, R. E. Jones, J. A. Barnett, R. H. Pratt, *Proc. IEE pt J.* **1985**, 132, 214.
8. G. V. Spillman, D. H. Mcmohan, *Appl. Phys. Lett.* **1980**, 37, 145.
9. S. Uena, *Bull. Japan Soc. Precision Engg.* **1973**, 7, 87.
10. K. Oki, T. Akihara, T. Shirai, *Powder Tech.* **1975**, 11, 51.
11. C. R. Tallman, F. P. Wingate, E. O. Ballard, *ISA Trans.* **1975**, 11, 19.
12. L. H. Lindstroem, *Biomed. Engg.* **1970**, BME-17, 207.
13. H. Matsumoto, M. Saegusa, K. Saito, K. Mizoi, *J. Med. Engg. Tech.* **1978**, 2, 239.
14. F. Parmigiani, *Opt. Quant. Electron.* **1978**, 10, 533.
15. S. Uena, N. Shibata, J. Tsujiuchi, *Opt. Com.* **1977**, 23, 407.
16. K. Kyuma, S. Tai, K. Hamanaka, M. Nuhoshita, *Appl. Opt.* **1981**, 20, 2424.
17. D. Marcuse, *Light Transmission Optics*. Van Nostrand Reinhold, New York, **1982**.
18. N. Lagakos, J. H. Cole, J. A. Bucaro, *Appl. Opt.* **1987**, 26, 2171.
19. Prerana, M. R. Shenoy, B. P. Pal, B. D. Gupta, *IEEE Sensors J.* **2012**, 12, 44.
20. A. Mignani, L. Ciaccheri, A. Cimato, G. Sani, *Sensors and Actuators B*, **2003**, 90, 157.
21. A. Kumar, T. V. B. Subrahmoniam, A. D. Sharma, K. Thyagarajan, B. P. Pal, I. C. Goyal, *Electron. Letts.* **1984**, 20, 534.
22. B. Nagaraju, R. K. Varshney, B. P. Pal, A. Singh, G. Monnom, B. Duusardier, *Proc. SPIE.* **2008**, 7138, 71381H1.
23. W. Johnstone, G. Thursby, D. Moodie, K. McCallion, *Opt. Lett.* **1992**, 17, 1538.
24. G. Raizada, B. P. Pal., *Opt. Lett.* **1996**, 21, 399.
25. T. G. Giallorenzi, J. A. Bucaro, A. Dandridge, A. Dandridge, G. H. Sigel, J. H. Cole, S. C. Rashleigh, R. G. Priest, *J. Quant. Electron.* **1982**, QE-18, 626.
26. A. Dandridge, Chapter on Fiber optic sensors based on the Mach-Zehnder and Michelson interferometers in *Fiber Optic Sensors: An Introduction for Engineers and Scientists*, ed. E. Udd, Wiley, New York, **1991**.
27. B. Culshaw, Chapter on Interferometric optical fiber sensors in *Fundamentals of Fiber Optics in Telecommunication and Sensor Systems*, ed. B. P. Pal, John Wiley, New York and Wiley Eastern, New Delhi, **1992**; latest reprint by New Age Publishers, New Delhi, **2014**.
28. B. P. Pal, Chapter on All-fiber components and devices in *Electromagnetic Fields in Unconventional Structures and Materials*, eds. A. Lakhtakia and O. N. Singh, John Wiley, New York, **2000**.
29. A. Ghatak, K. Thyagarajan. *Introduction to Fiber Optics*. Cambridge University Press, Cambridge, U.K., **1998**.
30. J. H. Cole, C. Kirkendall, A. Dandridge, G. Cogdell, T. G. Giallorenzi, *Washington Acad. Sc.* **2004**, 90, 40.
31. R. R. J. Maier, B. J. S. Jones, J. S. Barton, S. McCulloch, T. Allsop, J. D. C. Jones and I. Bennion, *J. Opt. Part A: Pure and Appl. Opt.* **2007**, 9, S45.
32. A. Trouillet, E. Marin, C. Veillas, *Meas. Sci. Technol.* **2006**, 17, 1124.
33. F. Silva, L. Coelho, O. Frazão, J. L. Santos, F. X. Malcata, *IEEE Sensors J.* **2012**, 12, 93.
34. Lee, B., Y. W. Lee, M. Song, Chapter on Principle and status of actively researched optical fiber sensors in *Guided Wave Optical Components and Devices: Basics, Technology and Applications*, ed. B. P. Pal, Academic Press/Elsevier, Burlington, MA, **2006**.
35. J. D. C. Jones, Chapter on Signal processing in monomode fiber optic sensor systems in *Fundamentals of Fiber Optics in Telecommunication and Sensor Systems*, ed. B. P. Pal, John Wiley, New York and Wiley Eastern, New Delhi, **1992**; latest reprint by New Age Publishers, New Delhi, **2014**.
36. D. W. Kim, Y. Zhang, K. L. Cooper, A. Wang, *App. Opt.* **2005**, 44, 5368.
37. P. L. Swart, *Meas. Sc. Tech.* **2004**, 15, 1576.
38. A. V. Brakel, P. L. Swart, *Opt. Engg.* **2005**, 44, 1576.
39. K. S. Park, H. Y. Choi, S. J. Park, U. C. Paek, B. H. Lee, *IEEE Sensors Journal*, **2010**, 10, 1147.
40. S. Ezekiel, H. J. Arditty, Chapter on Fiber optic rotation sensors: Tutorial review in *Fiber-Optic Rotation Sensors and Related Technologies*, eds. S. Ezekiel, H. J. Arditty, Springer-Verlag, Berlin, Germany, **1982**.
41. V. Vali, R. W. Shorthill, *App. Opt.* **1976**, 15, 1099.
42. E. Udd, Chapter on Overview of fiber optic sensors in *Fiber Optic Sensors*, eds. F. T. S. Yu, S. Yin, Marcel Dekker, New York, **2002**.
43. H. Y. Fu, H. Y. Tam, L. Y. Shao, X. Y. Dong, P. K. A. Wai, C. Lu, S. K. Khijwani, *Appl. Opt.* **2008**, 47, 2835.
44. D. S. Moon, B. H. Kim, A. Lin, G. Sun, Y. -G. Han, W.-T. Han, Y. Chung, *Opt. Exp.* **2007**, 15, 7962.
45. G. Kim, T. Cho, K. Hwang, K. Lee, K. S. Lee, Y. G. Han, S. B. Lee, *Opt. Exp.* **2009**, 17, 2481.
46. J. M. Baptista, J. L. Santos, A. S. Lage, *Opt. Comm.* **2000**, 181, 287.
47. P. Zu, C. C. Chan, Y. Jin, T. Gong, Y. Zhang, L. H. Chen, X. Dong, *Photon. Techn. Lett.* **2011**, 23, 920.
48. B. Dong, J. Hao, C. Y. Liaw, Z. W. Xu, *J. Lightwave Tech.* **2011**, 29, 1759.

49. O. Frazao, J. M. Baptista, J. L. Santos, P. Roy, *Appl. Opt.* **2008**, *47*, 2520.
50. H. F. Taylor, Chapter on Fiber optic sensors based upon the Fabry–Perot interferometer in *Fiber Optic Sensors*, eds. F. T. S. Yu, S. Yin, Marcel Dekker, New York, **2002**.
51. B. H. Lee, H. Y. Kim, K. S. Park, J. B. Eom, M. J. Kim, B. S. Rho, H.Y. Choi, *Sensors*. **2012**, *12*, 2467.
52. X. Wan, H. F. Taylor, *Opt. Letts.* **2002**, *27*, 1388.
53. Z. Wang, F. Shen, L. Song, X Wang, A. Wang, *Photon. Tech. Lett.* **2007**, *19*, 1388.
54. Z. Ran, Y. Rao, J. Zhang, Z. Liu, B. Xu, *J. Lightwave Tech.* **2009**, *27*, 5426.
55. Z. L. Ran, W. J. Rao, X. Liao, X. Liao, K. S. Chiang, *Opt. Exp.* **2008**, *16*, 2252.
56. V. R. Machavaram, R. A. Badcok, G. F. Fernando, *Sensors and Actuators*. **2007**, *A 138*, 248.
57. A. D. Kersey, D. Jackson, M. Corke, *Opt. Comm.* **1983**, *45*, 71.
58. S. J. Petuchowski, T. G. Giallorenzi, S. K. Sheem, *J. Quant. Electron.* **1981**, *17*, 2168.
59. T. Yoshino, K. Kurosawa, T. Ose, *IEEE J. Quant. Electron.* **1982**, *18*, 1624.
60. C. E. Lee, H. F. Taylor, *Electro. Lett.* **1988**, *24*, 193.
61. T. A. Tran, W. V. Miller III, K. A. Murphy, A. M. Vengsarkar, R.O. Claus, *Proc. SPIE.* **1991**, *1584*, 178.
62. F. Mitschke, *Opt. Lett.* **1989**, *14*, 967.
63. T. Li, A. Wang, K. Murphy, R. Claus, *Opt. Lett.* **1995**, *20*, 785.
64. M. D. Barrett, E. H. Peterson, J. W. Grant, *IEEE Trans. Biomed. Engg.* **1999**, *46*, 331.
65. K. D. Oh, J. Ranade, V. Arya, A. Wang, R. O. Claus, *Phot. Tech. Lett.* **1997**, *9*, 797.
66. W. Jin, T. K. Y. Lee, S. L. Ho, H. L. Ho, K. T. lao, L. M. Zhao, Y. Zhao, Chapter on Structural strain and temperature measurements using fiber Bragg grating sensors, in *Guided Wave Optical Components and Devices: Basics, Technology, and Applications*, ed. B. P. Pal, Academic Press/Elsevier, Burlington, MA, **2006**.
67. M. Measures, *Structural Monitoring with Fiber Optic Technology*. Academic Press, London, U.K., **2001**.
68. A. Orthonos, K. Kalli, *Fiber Bragg Gratings: Fundamentals and Applications in Telecommunication and Sensing*, Artech House, Boston, MA, **1999**.
69. A. D. Kersey, M. A. Davies, H. J. Patrick, M. LeBlanc, K. P. Koo, C. G. Askins, M. A. Putnam, E. J. Friebele, *J. Lightwave Tech.* **1997**, *15*, 1442.
70. A. Cusano, P. Capoluongo, S. Campopiano, A. Cutolo, M. Giordano, F. Felli, A. Paolozzi, M. Caponero, *IEEE Sensors J.* **2006**, *6*, 67.
71. U. Ben-Simon, I. Kressel, Y. Botsev, A. K. Green, G. Ghilai, N. Gorbatov, M. Tur, S. Gali, *Proc. SPIE.* **2007**, *6619*, 661944.
72. B. P. Pal, *Asian J. Phys.* **2003**, *12*, 263.
73. M. Majumdar, T. K. Gangopadhyay, A. K. Chakraborty, K. Dasgupta, D. K. Bhattachary, *Sensors and Actuators A*, **2009**, *150*, 78.
74. T. K. Gangopadhyay, Personal communication, CGCRI, Kolkata, India, **2012**.
75. K. Bløtekjær, Chapter on Fiber optic sensor multiplexing in *Fundamentals of Fiber Optics in Telecommunication and Sensor Systems*, ed. B. P. Pal, John Wiley, New York and Wiley Eastern, New Delhi, **1992**; latest reprint by New Age Publishers, New Delhi, **2014**.
76. B. Culshaw, *IEEE J. Lightwave Tech.*, **2004**, *22*, 39.
77. I. Perez, C. Hong-Liang, E. Udd, *Proc. SPIE.* **2001**, *2007*, 209.
78. T. K. Gangopadhyay, M. Paul, L. Bjerkan, *Proc. SPIE.* **2009**, *7503*, 75034M01.
79. A. M. Vengsarkar, P. J. Lemaire, J. B. Judkins, *J. Lightwave Tech.*, **1996**, *14*, 58.
80. Bhatia, V., A. M. Vengsarkar, *Opt. Lett.* **1996**, *21*, 692.
81. V. Bhatia, *Opt. Exp.* **1999**, *4*, 457.
82. Sanders, J. L. Blake, A. H. Rose, F. Rahmatian, C. Herdman, *The 15th Optical Fiber Sensors Conference Technical Digest*, **2002**, Portland, OR, p. 31.
83. A. L. Rogers, Chapter on Optical fibers for power systems in *Fundamentals of Fiber Optics in Telecommunication and Sensor Systems*, ed. B. P. Pal, John Wiley, New York and Wiley Eastern, New Delhi, **1992**; latest reprint by New Age Publishers, New Delhi, **2014**.
84. A. J. Rogers, *Int. J. Optoelectron.* **1988**, *3*, 391.
85. R. Ulrich, A. Simon, *Appl. Opt.* **1979**, *18*, 2241.
86. F. Briffod, D. Alasia, L. Thevenaz, *The 15th Optical Fiber Sensors Conference, Tech. Dig.* **2002**, Portland, OR, Post-deadline paper PD3.
87. L. Grant, G. Schoetz, J. Vydra, D. G. Fabricant. *Proc. SPIE.* **1998**, *3355*, 884.
88. P. R. Carey. *Biochemical Applications of Raman and Resonance Raman Spectroscopy*. Academic, New York, **1982**.
89. J. F. Brennan III, W. Yang, R. R. Dasari, M. S. Feld. *Appl. Spectrosc.* **1997**, *51*, 201.
90. X. -D Wang, O. S. Wolfbeis. *Anal. Chem.* **2013**, *85*, 487.
91. Lee C. L. Chin, William M. Whelan, I. Alex Vitkin, Chapter on Optical Fiber Sensors for Biomedical Applications in *Optical-Thermal Response of Laser-irradiated Tissue.*, Eds. A. J. Welch, van Gemert, J. C. Martin, Springer eBook, **2011**.
92. Y. Sun, J. Phipps, D. S. Elson, H. Stoy, S. Tinling, J. Meier, B. Poirier, F. S. Chuang, D. G. Farwell, L. Marcu, *Opt. Lett.* **2009**, *34*, 2081.
93. U. Utzinger, R. R. Richards-Kortum, *J. Biomed. Opt.* **2003**, *8*, 12.
94. D. Huang, E. A. Swanson, C. P. Lin, J. S. Schuman, W. G. Stinson, W. Chang, M. R. Hee, T. Flotte, K. Gregory, C. A. Puliafito, J. G. Fujimoto, *Science* **1991**, *254*, 1178.
95. H. Li, B. A. Standish, A. Mariampillai, N. R. Munce, Y. Mao, S. Chiu, N.E. Marcon, B.C. Wilson, A. Vitkin, V. X. Yang, *Lasers Surg. Med.* **2006**, *38*, 754.
96. O. Frazão, M. S. Ferreira, R. M. André, S. O. Silva, M. B. Marques, José L. Santose, *Optical Sensors, Advanced Photonics Conference*, **2014**, Barcelona, Spain, Paper SeW3C.



Bishnu P. Pal obtained M.Sc. and Ph.D. degrees in Physics from Jadavpur University (Kolkata) and IIT Delhi in 1970 and 1975 respectively, as a National Science Talent Search Scholar. In late 1977 he joined the academic staff of IIT Delhi as a specialist on Fiber Optics, where he served as Professor of Physics since 1990 till his retirement. Recently he joined the faculty of Mahindra Ecole Centrale at Hyderabad. He has worked in the area of Fiber Optics and Applications for various periods at the Norwegian Institute of Technology (Norway), the Fraunhofer Institute für Physikalische Messtechnik, Freiburg (Germany) as an AvH Fellow, National Institute of Standards and Technology, Boulder (USA) as a Fulbright Scholar, Heriot-Watt University, Edinburgh, UK as Erasmus Mundus Fellow in Photonics, and as Guest Professor at Optoelectronics Research Center at City University of Hong Kong, and University of Nice (France) for various periods. Prof. Pal has extensive teaching, research, sponsored R&D, and consulting (for Indian and US industries) experience on various aspects of Fiber Optics and related components, and he has published and reported over 180 research papers and research reviews in international journals and conferences, and has coauthored one each Indian and US patents. He has edited several semi-text/reference books on Photonics and has also contributed 15 book chapters. He was deeply involved with the conception and development of the

Fiber Optics Laboratory at IIT Delhi in late 1970s. Prof. Pal is a Fellow of OSA The Optical Society (USA), Honorary Foreign Member of the Royal Norwegian Academy of Sciences and Letters (Norway), and is a Senior Member of IEEE. He has been an invited speaker at 50 international conferences, and a Chair/Member of the Technical/Advisory Committees of several International Conferences in India and abroad. He is a recipient of the Homi Bhabha Award of UGC in Applied Sciences, Om Prakash Bhasin Award in Electronics and Information Technology, Prof Y T Thathachari award of Bhramara Trust (Mysore), IEEE Photonics Society's Distinguished Lecturer (2005–2007) Khosla Research award for life time achievements from IIT Roorkee for 2014, a co-recipient (with K. Thyagarajan) of the *First Fiber Optic Person of the Year award* in 1997 instituted by Lucent Technology in India for his significant contributions in all-fiber components for optical networks besides several other awards. His current research interest is in guided wave optical components for DWDM and optical networks, Mid-IR Photonics, specialty fibers like Microstructured fibers, Nonlinear Fiber Optics, silicon photonics, fiber optic sensors, and transverse localization of light in a disordered optical waveguide lattice. He was member of the Board of Directors of OSA The Optical Society (2009–2011), and is currently President of Optical Society of India since 2012, as well as an Associate Vice President of Membership Council of IEEE (USA) since 2012.

